AGU PUBLICATIONS

JGR

Journal of Geophysical Research: Earth Surface

RESEARCH ARTICLE

10.1002/2013JF002933

Key Points:
- Repeat aerial lidar is used to quantify fluvial sediment transport
- Two total sediment loads and streamflow used to create a sediment rating curve
- Methods provide estimates of transport rates in steep streams

Correspondence to:
S. Anderson,
scott.w.anderson@colorado.edu

Citation:
Anderson, S., and J. Pitlick (2014), Using repeat lidar to estimate sediment transport in a steep stream, *J. Geophys. Res. Earth Surf.*, *119*, 621–643, doi:10.1002/2013JF002933.

Received 25 JUL 2013
Accepted 7 FEB 2014
Accepted article online 13 FEB 2014
Published online 26 MAR 2014

Using repeat lidar to estimate sediment transport in a steep stream

Scott Anderson[1] and John Pitlick[1]

[1]Department of Geography, University of Colorado Boulder, Boulder, Colorado, USA

Abstract Sediment fluxes in steep mountain streams remain difficult to quantify, despite their importance in geomorphology, ecology, and hazard analysis. In this work, aerial lidar surveys, acquired in 2002, 2008, and 2012, are used to quantify such fluxes in Tahoma Creek, a proglacial stream on Mount Rainier, Washington. As these surveys encompass all coarse sediment sources in the basin, we are able to translate geomorphic change into total bed material transport volumes for the time steps between surveys. By assuming that the relationship between daily sediment transport and daily mean discharge is of the form $Q_s = a(Q - Q_c)^b$, our two observed total loads and estimates of daily mean discharge allow us to numerically solve for values of a and b to create a bed material sediment rating curve. Comparisons of our transport estimates with sediment deposition in a downstream reservoir indicate that our transport estimates and derived rating curve are reasonable. The method we present thus represents a plausible means of estimating transport rates in energetic settings or during extreme events, applicable whenever at least two cumulative sediment loads and the driving hydrology are known. We use these results to assess the performance of several bed load transport equations. The equations generally overpredict transport at low to moderate flows but significantly underpredict transport rates during an extreme event. Using a critical shear stress value appropriate for steep streams improves agreement at lower flows, whereas a shear-partitioning technique accounting for form drag losses significantly underpredicts transport at all flows.

1. Introduction

Steep mountain streams are energetic systems that transport significant volumes of sediment and are often the source of the majority of the coarse sediment load within a basin. Sediment fluxes in these environments are an integral part of the transfer of sediment from source areas to depositional settings, and so they influence bedrock incision rates [*Sklar and Dietrich*, 2004], channel morphology, and flood hazards [*Czuba et al.*, 2012a] and are a necessary piece of information in various river engineering and restoration activities. The intense rates of transport may also constitute a significant natural hazard for local communities and infrastructure. To date, predicting mountain stream sediment fluxes remains difficult. Our current understanding of sediment transport, developed primarily in low-gradient rivers and laboratory flumes, does not necessarily transfer to these environments, and sediment transport equations often mispredict transport rates by several orders of magnitude [*Rickenmann*, 2001]. This poor performance has been variously explained as a failure to account for the increased form drag losses in steeper streams [*Chiari and Rickenmann*, 2007; *Nitsche et al.*, 2011] or the increasing critical shear stresses observed with increasing slopes [*Mueller et al.*, 2005; *Lamb et al.*, 2008]. More broadly, the relative lack of accurate measurements of sediment transport rates in steep streams hampers our ability to develop empirical relations for these environments. Direct measurements of sediment transport, and particularly the geomorphically significant bed material fraction, are complicated by the energetic transport of coarse sediment and the logistical difficulties of making such measurements at remote sites during episodic events.

In recent decades, the increased resolution and availability of topographic surveys has presented the possibility of quantifying sediment fluxes through the analysis of repeat measurements. This method, referred to as morphologic budgeting, assumes that sufficiently accurate measurements of landscape change should provide estimates of accumulated transport rates, given simple conservation of mass. The idea is not a new one, having been suggested in the context of fluvial transport as early as the early 1960s and 1970s [*Popov*, 1962; *Neill*, 1971] and used with some success along the Fraiser River in the late 1990s [*McLean and Church*, 1999]. However, modern survey techniques have significantly increased the potential accuracy and extent of morphologically based transport estimates and have recently been used to quantify fluxes in landslides

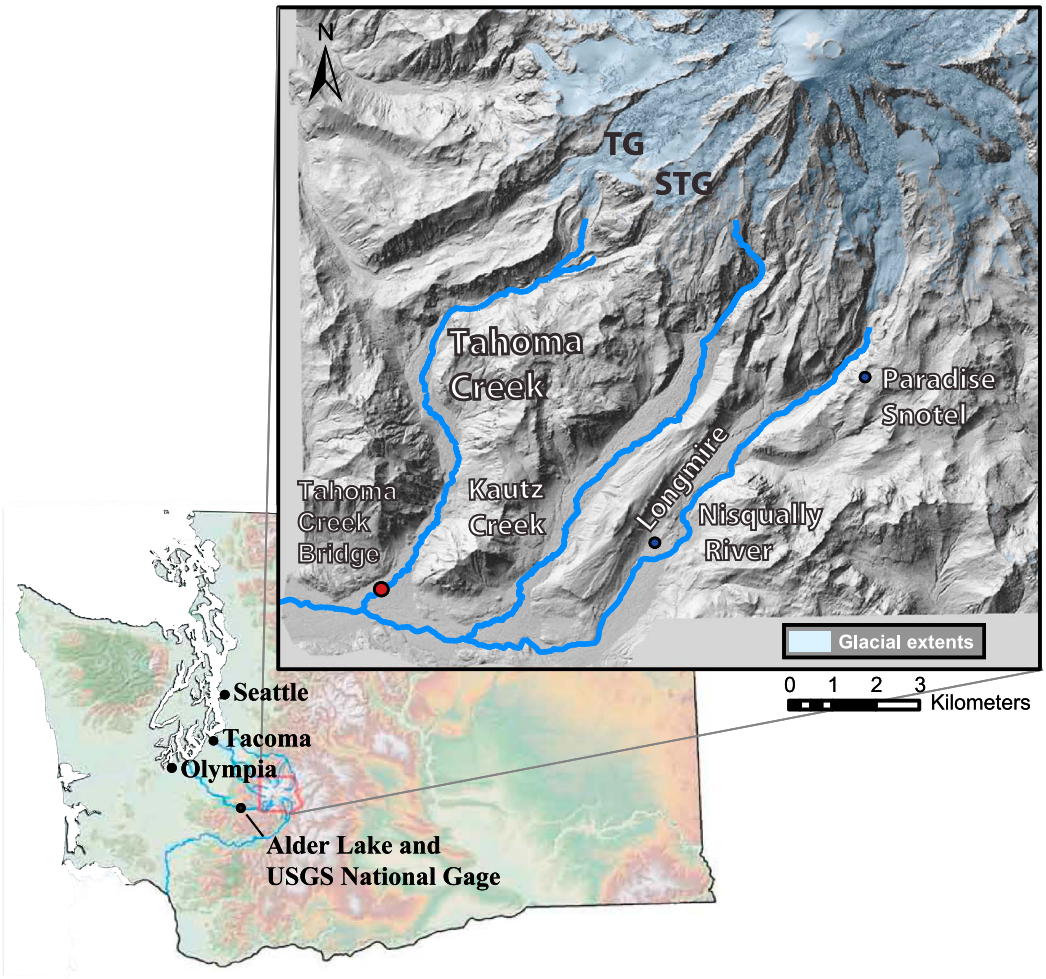

Figure 1. Map showing regional location of Mount Rainier, with inset showing the southern flank of the mountain, where Tahoma Creek is located. Glacier extents based on 2008 lidar and taken from *Robinson et al.* [2010]. The Tahoma Glacier and South Tahoma Glacier are labeled TG and STG, respectively. Various locations referenced in the text are indicated.

[*DeLong et al.*, 2012], debris flows [*Schürch et al.*, 2011], and fluvial transport [*Lane et al.*, 2003; *Wheaton et al.*, 2010; *Croke et al.*, 2013]. These methods are particularly well suited to the quantification of transport in energetic settings or during extreme events, in which the scale of geomorphic change is generally large and where more direct measurements of transport are often inaccurate, unsafe, or otherwise untenable.

In this work, we present an application of morphologic budgeting methods in which repeat aerial lidar surveys are used to estimate sediment fluxes down the length of Tahoma Creek, a steep, proglacial stream located on the southwest flank of Mount Rainier, Washington (Figure 1). We use surveys acquired in 2002, 2008, and 2012 to estimate accumulated volumetric transport over the two time intervals between surveys, the earlier of which includes the effects of a massive flood in November 2006. We then present a method by which these accumulated loads, in combination with discharge records, may be used to estimate sediment rating curves. This is accomplished by noting that our accumulated transport volumes can be described as the integral of transport rates over the relevant time periods and, in turn, that transport rates may be described as a monotonic, continuous function of discharge. With two independent time periods, we are able to write two equations of the form $\mathrm{AL} = \int_{t_1}^{t_2} f(Q)$, where AL is the accumulated sediment load measured from our lidar surveys and $f(Q)$ is an unspecified function describing the relationship between discharge and sediment transport rate. Positing that $f(Q)$ takes the form of a power law, aQ^b, we can use these two equations to numerically solve for the unique values of a and b that correctly predict our lidar-derived estimates of accumulated transport over both time periods. These values of a and b then provide temporarily continuous estimates of transport rates at the resolution of our discharge records and may

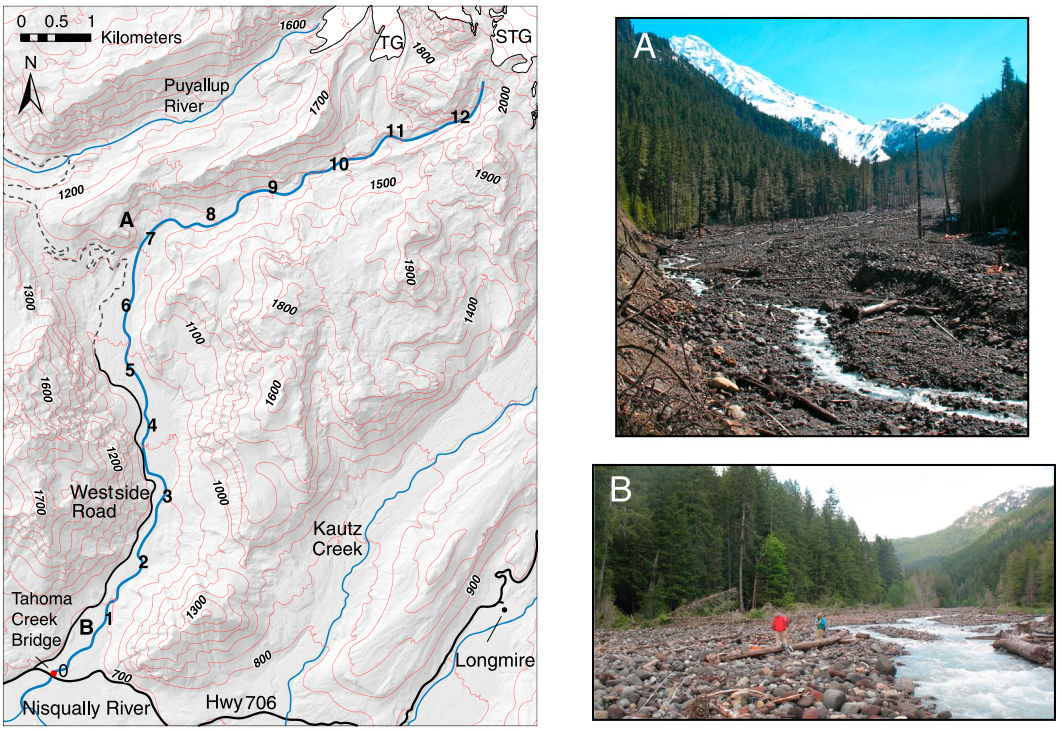

Figure 2. Map of Tahoma Creek, with bold numbers along valley indicating distance upstream from the Tahoma Creek Bridge in kilometers, measured along the valley centerline. (a) Photo looking upstream toward the upstream extent of debris flow deposition. (b) A representative view of the downstream, fluvial reach of Tahoma Creek. Locations of Figures 2a and 2b are indicated on the map.

be used to estimate transport for time periods outside of our survey intervals. Finally, we use both our estimates of accumulated transport and our derived rating curve to assess the skill of several bed load transport equations applied to the steep settings of Tahoma Creek.

We present these analyses in two broad sections: the first entails the methods and results of our lidar analysis, as well as an assessment of those results, and the second section then presents the methods by which we used our lidar results to assess transport equations and the results of that assessment. The subsequent discussion and conclusions encompass both sections.

2. Study Area

The focus of this study is Tahoma Creek, a 38 km^2 basin draining the southwest flank of Mount Rainier (Figure 1). Locations within the study area are noted as the number of kilometers upstream from the Tahoma Creek Bridge (Figure 2) traced along a valley centerline and indicated as valley kilometers (VK) in the remainder of the text.

Tahoma Creek is sourced primarily from the South Tahoma Glacier, with minor contributions from a tongue of the Tahoma Glacier. In its uppermost 2 km, the stream flows through unconsolidated neoglacial sediment, which provide much of the coarse sediment load for the river. These sediments are commonly mobilized by debris flows. The channel enters a confined reach between VKs 8 and 9, after which the valley widens significantly. Debris flow deposition is focused within this wider reach, between VKs 5 and 8. Below VK 5, fluvial processes dominate. Tahoma Creek flows into the Nisqually River at VK −0.5, just downstream of the Tahoma Creek Bridge. In the lower reaches, the stream is primarily single-thread with zones of mild braiding, flowing through an active channel 30 to 70 m wide. This active channel is composed primarily of bare gravel, hosting occasional alder stands. The channel is bordered by a 2 to 3 m high terrace surface, supporting extensive conifer forests. Channel slopes range between 0.1 and 0.3 in the source area above VK 9, between 0.06 and 0.1 in the debris flow deposition zone between VKs 5 and 9, and between 0.03 and 0.045 in the lower fluvial reach below VK 5.

Table 1. Comparison of Alder Lake Sedimentation Rates With Predicted Bed Material Transport in Tahoma Creek

Reference Year	Operator	Flight Dates	All-Return Point Density (pt/m^3)[a]	Ground-Return Point Density (pt/m^3)[a]	Survey Coverage	Data Location
2002	Terrapoint	Dec 2002	2.57	0.77	Above VK 1.3	Not publically available
2008	Watershed Sciences	Sept 2008	7	0.7–2	Entire basin	Available through Puget Sound LiDaR Consortium http://pugetsoundlidar.ess.washington.edu/lidardata/index.html
2012	National Center for Aerial Laser Mapping (NCALM)	Aug 2012	4.97	3.78	Entire basin	Available through Open Topography: DOI: 10.5069/G9PZ56R1

[a]Point densities for 2002 and 2012 surveys taken from original point clouds, clipped to the area of analysis. Densities for 2008 flight are averages for entire survey, presented in the survey report.

Tahoma Creek has generated a significant number of debris flows, with 27 recorded events over the past 40 years. The majority of these events occurred during two concentrated periods, the first between 1967 and 1972 and the second between 1986 and 1992. *Walder and Driedger* [1994a] concluded that outburst floods from South Tahoma Glacier were the most likely triggers for the debris flows between 1986 and 1992.

3. Methods—Analysis of Repeat Lidar

This analysis centers on three sets of aerial lidar acquired in 2002, 2008, and 2012. The two later data sets cover the entire length of Tahoma Creek, from the glacial source to its confluence with the Nisqually River, while the 2002 data set has coverage only above VK 1.3. All analyses were performed using derived 1 m bare-earth digital elevation models (DEMs), with ground classification and raster interpolation performed by the survey operators. Technical details of these surveys are noted in Table 1. After ensuring that the data sets were in the same horizontal coordinate system and aligned to the same vertical datum, we did the following:

1. Created 2008–2002 and 2012–2008 DEMs of difference (DoDs);
2. Summed volumetric change upstream of a point to estimate bed material transport past that point, under the assumption that the lidar captures all sources and sinks of bed material and that sediment may only exit the valley through downstream motion;
3. Used these estimates of total bed material transport, as well as flow records for the basin, to produce a simple sediment rating curve that allows us to predict total daily bed material transport as a function of discharge.

3.1. Coordinate System and Vertical Datum Alignment

We projected all three original bare-earth DEMs into North American Datum 83 Universal Transverse Mercator coordinates, using the North American Vertical Datum 88 vertical datum and converted to orthometric elevations using GEOID03. All three surveys were georeferenced using independent GPS monuments and so contained residual offsets at the scale of GPS uncertainty (±10 cm). We used terrain-matching techniques to detect and remove these offsets to the best of our abilities, described below. Because change analysis depends only on the relative alignment of the data sets, we chose the 2008 survey as our "ground truth," as it covered the largest spatial extent and fully overlapped with both the 2002 and 2012 surveys. We then aligned the 2002 and 2012 data sets to that baseline.

Horizontal alignments were evaluated by first isolating areas presumed to be geomorphically stable over the survey intervals and then calculating apparent change in these areas as a function of aspect, conceptually similar to the method presented in *DeLong et al.* [2012]. Horizontal offsets create a sinusoidal pattern in the resulting plot of mean change versus aspect, with the peak/trough indicating the direction of the offset. Both the 2002 and 2012 data sets contained apparent offsets on the order of 0.15 m. These were corrected to the best of our abilities, though horizontal offsets on the scale of centimeters likely still exist. The 2002

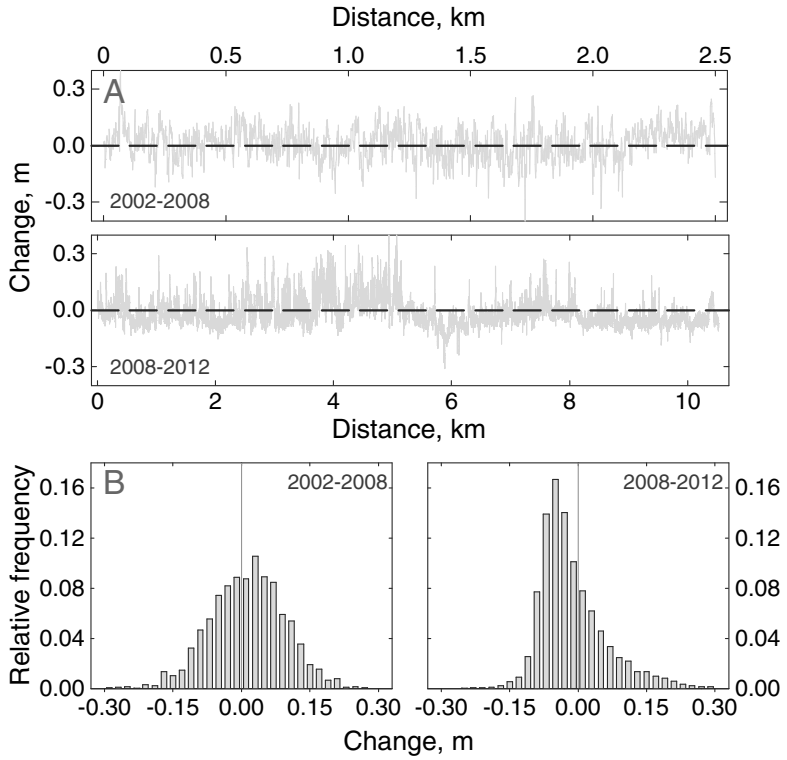

Figure 3. (a) Long profiles of apparent change along the Westside Road, taken after vertical datum offsets were removed to the best of our abilities. Distance is in kilometers, measured along the roadway, with a sampling density of one point per meter. The 2008–2012 survey encompasses more of the Westside Road as it leaves the Tahoma Creek basin and so provided more length for comparison. (b) Histograms of values shown in long profile plots in Figure 3a.

and 2012 rasters were then snapped and resampled to overlap exactly with the 2008 grid. Vertical datum offsets were estimated by comparing bare, level surfaces along the Westside Road (Figures 2 and 3). After correcting a 0.04 m offset found in the 2012 data set, we measured an unresolved mean offset between the 2002 and 2012 road surfaces of 0.015 m. We use this offset to conservatively estimate our vertical datum uncertainty at 0.025 m and use this value in our quantification of uncertainty below. Sequential data sets were then subtracted to create two DoDs, one representing change from December 2002 to September 2008 and one representing change from September 2008 to September 2012 (Figures 4 and 5). DoDs were created by subtracting the earlier data set from the later, such that aggradation produced positive numbers.

We restricted our analysis to the lateral moraines at the head of the valley and the active valley floor downstream, ignoring the forested valley walls. Both the lidar itself and observations made in the field suggest that these valley walls contribute minimal sediment to the basin, as there was no evidence of mass movement or deltas at tributary junctions. Lidar noise was significantly larger and point densities lower over these valley walls as well, such that inclusion in the analysis would likely increase uncertainty while changing our estimates of total volumetric change only minimally.

The skewed distribution of apparent change measured along the Westside Road in Figure 3b for the 2008–2012 period is likely the result of how strict the survey operators were when classifying ground points within the all-return point cloud. The National Center for Aerial Laser Mapping (NCALM) notes that they chose a less strict classification process in their 2012 survey than what was likely used in the 2008 Watershed Sciences survey [*NCALM*, 2012]. Although the road is not obscured by significant vegetation (with the exception of the overhanging canopy, which should be readily removed by either classification scheme), there will still be some level of local variations in the road elevation (both real and as a product of survey noise). Presumably, a stricter ground point classification scheme would be more likely to remove some of the anomalous high points. Removal of these high points effectively lowers the mean surface elevation slightly. However, as our method for detecting vertical datum offsets is based on comparisons of those mean surface elevations, our manually aligned surfaces should be in rough agreement.

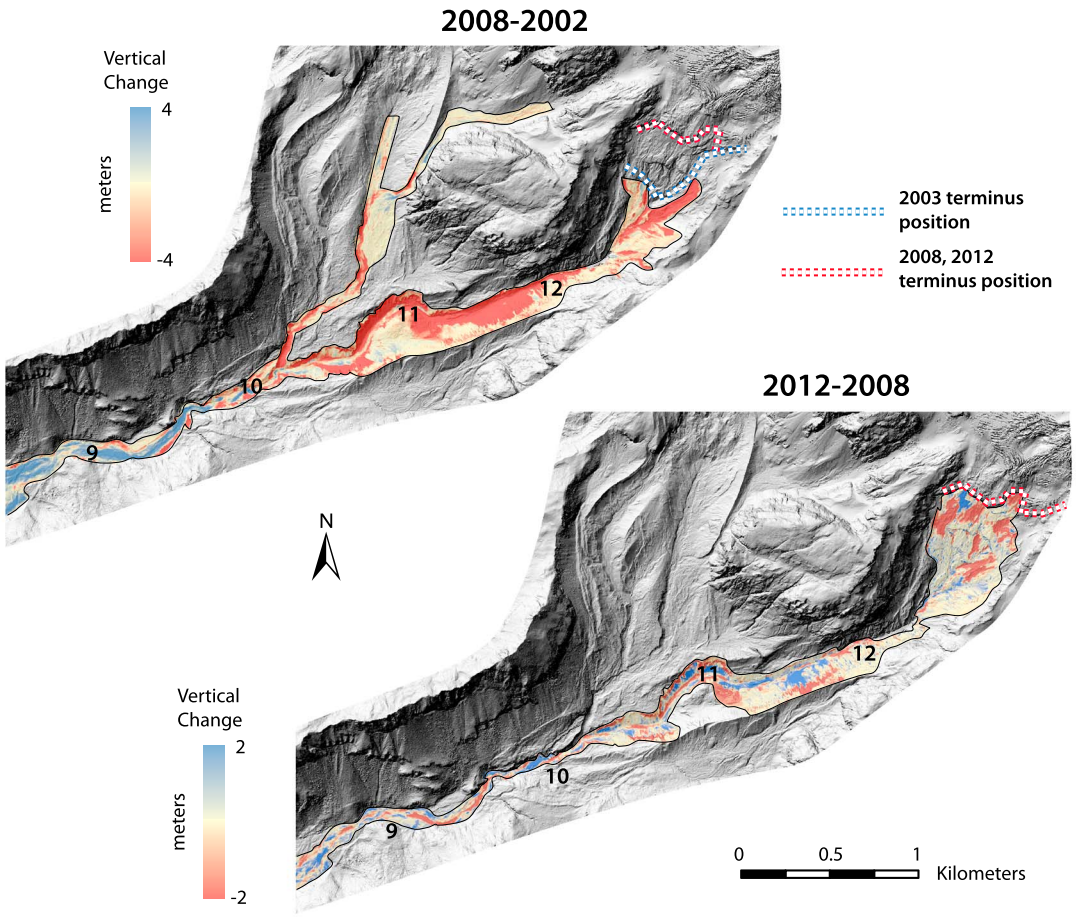

Figure 4. Vertical change in the upper basin of Tahoma Creek. Change is shown only over the area of analysis, overlaid on the 2012 bare-earth hillshade. Aggradation is positive and indicated by blue shades, and incision is negative and indicated by red shades. Numbers indicate kilometers upstream from the Tahoma Creek Bridge, as measured along the valley centerline. Approximate positions of the South Tahoma Glacier terminus in 2002, 2008, and 2012 are indicated. Note that the color ramps used to indicate change differ between 2002–2008 and 2008–2012, as the magnitude of change differed appreciably between the two time periods.

3.2. Quantification of Survey Uncertainty

The topographic surveys we use to quantify change are inherently subject to some level of uncertainty. We divide this uncertainty into two sources: spatially variable uncertainty and vertical datum uncertainty. Spatially variable uncertainty is a function of noise, presumed to be white noise, operating at the level of individual observations, while vertical datum uncertainty represents the confidence that two data sets are referenced to the same vertical datum. Although datum uncertainties may also exist in the horizontal, in the relatively low-slope fluvial environments we are interested in, vertical uncertainties more directly impact apparent volumetric change. We denote these uncertainties as normal distributions with means of zero and standard deviations σ_{sv} and σ_{vd}, respectively. Of the two, spatially variable errors have received a majority of the attention in past works, with numerous attempts to quantify σ_{sv} and explore how that value may vary across a landscape [*Wheaton et al.*, 2010; *Milan et al.*, 2011]. These estimates often constitute a basis for defining a threshold of detection—changes smaller than some value are considered indistinguishable from noise and so are excluded from the analysis [e.g., *Croke et al.*, 2013]. Such techniques could be considered bottom-up methods, in that they attempt to describe the uncertainty around individual observations and propagate that uncertainty forward when making estimates of volumetric change. We present here instead a top-down approach to quantifying uncertainty, in which we first calculate the sum of volumetric change over the landscape (our final quantity of interest) and then attempt to put uncertainty bounds on this value as a function of σ_{sv} and σ_{vd} using simple parametric statistics. Although such an approach is less typical and

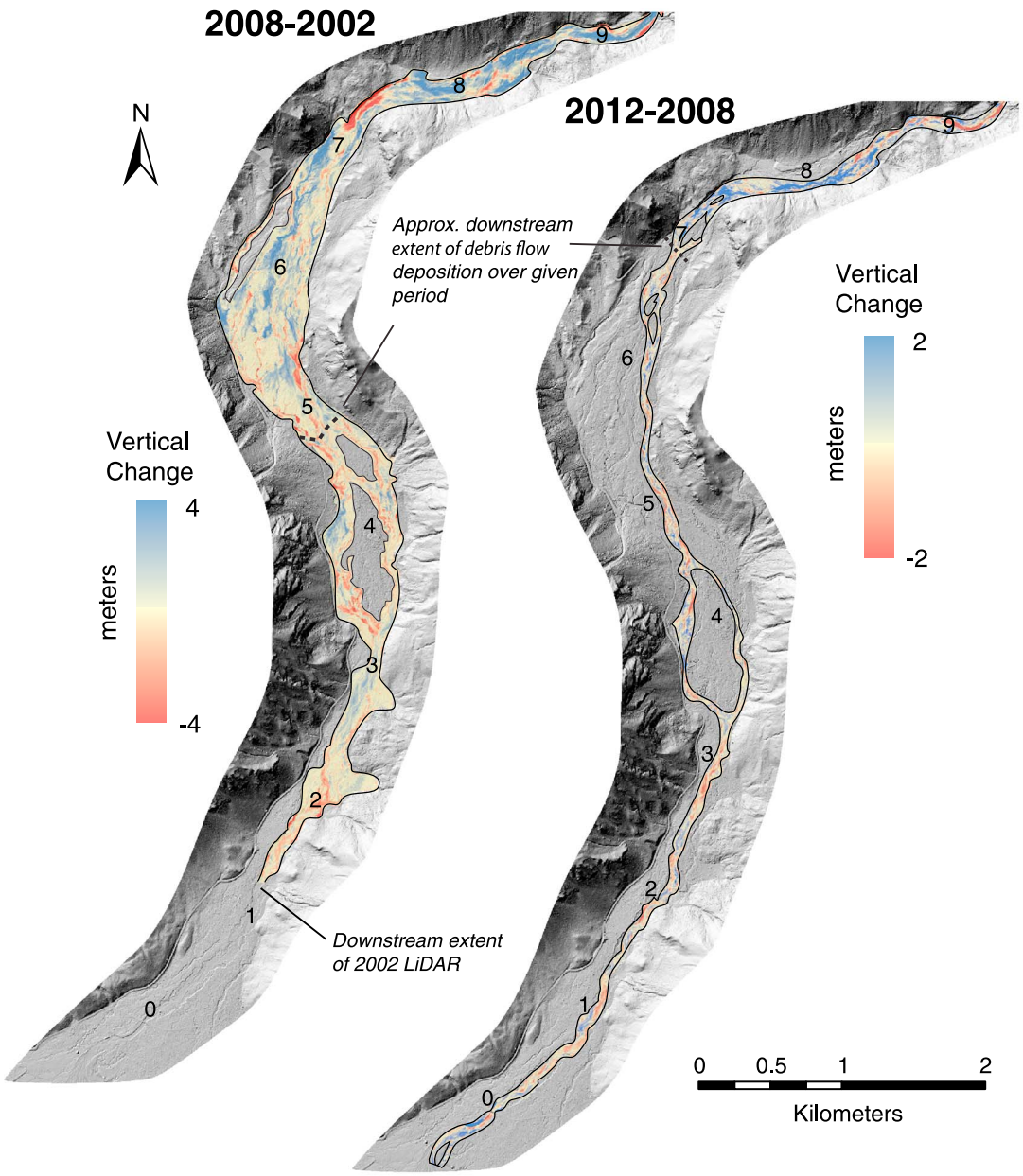

Figure 5. Lidar-derived DEMs of difference showing change in the lower Tahoma Creek basin. Format is the same as in Figure 4. The approximate downstream extent of debris flow deposition is noted for each time period. The greater distance of debris flow deposition shown for the 2002–2008 time period corresponds to the downstream limit of debris flow deposition observed in recent decades.

certainty more simplistic than many of the error models currently available, we found it to be a useful way of approaching uncertainty in our specific data sets and in regards to our specific research goals. In these calculations, we discuss directly the uncertainty in a derived DoD, noting that the spatially variable uncertainty of the two parent surveys, σ_a and σ_b, combine such that $\sigma_{sv} = \sqrt{\sigma_a^2 + \sigma_b^2}$.

We begin with the purely statistical statement that the mean value of n observations pulled from a normal distribution approximates the true mean with an uncertainty defined by the standard error of the mean,

$$\frac{\sigma}{\sqrt{n}}. \quad (1)$$

By extension, the sum of n observations pulled from a normal distribution approximates the expected sum, $n\mu$, with an uncertainty

$$\frac{\sigma}{\sqrt{n}}n = \sigma\sqrt{n}, \tag{2}$$

a value we refer to here as the standard error of the summation. Summing normally distributed random values is what occurs when spatially variable errors are summed in volumetric estimates of change. The standard error of summation thus provides a metric of the uncertainty associated with spatially variable errors in regards to net volumetric change. If, as we presume, the true mean is zero, the area-normalized uncertainty (m^3/m^2) should decrease with n, the number of observations.

In the case of lidar surveys, n would most properly be given as the number of independent *xyz* points. However, to provide more physically intuitive results, we choose to use the number of cells in a raster. In the case of the 1 m DEMs we use here, this is equivalent to the area in square meters. Given that our surveys have point densities of ~1 pt/m^2, the two values produce similar results. The relevant standard deviation is that of the spatially variable uncertainty, σ_{sv}. Using these values, the standard error of the summation then becomes a direct estimate of the volumetric uncertainty that spatially variable uncertainties contribute in a summation of volumetric change. That the equation appears to provide a quantity with units of area, and not volume, is a result of the fact that n is both the number of observations and the area in square meters; although they are numerically equivalent in our case of 1 m DEMs, the former is dimensionless, while the latter has units of area. A more physically intuitive way of demonstrating that this value is indeed a volume can be arrived at by first considering the standard error of the mean of spatially variable errors. This value has units of length. Multiplying this length scale, which describes the residual error one would expect after high and low errors offset each other to some degree, by the area of analysis thus gives a volumetric quantity. Note that this value is independent of measured change, being a function of only the magnitude of noise in the survey and survey area.

It is possible to logically extend this analysis to rasters of any cell size, as long as the assumption of ~1 pt/cell is reasonable. In the case of a DEM with cell length L

$$\frac{\sigma_{sv}}{\sqrt{n}}nL^2 = \sigma_{sv}\sqrt{n}L^2 \tag{3}$$

provides a direct estimate of volumetric uncertainty in the sum of volumetric change. That this is equivalent to equation (2) can be seen by setting $L = 1$.

Vertical datum uncertainty errors are presumed to operate everywhere in the same direction with the same magnitude. Thus, the total volumetric uncertainty is simply σ_{vd} times the area of analysis.

3.3. Application to This Study

To estimate σ_{sv} for our DoDs, we first examined the standard deviation of apparent change along the Westside Road, as seen in Figure 3. For both time periods, $\sigma_{sv} = 0.08$ m. This is likely an underestimate of σ_{sv} over more topographically complex areas, such as the cobble- and boulder-strewn channel we are interested in, and we conservatively increase this number to 0.3 m. Using our total area of analysis (1.5×10^6 m^2), equation (2) predicts that spatially variable errors would contribute $\pm$350 m^3 of volumetric uncertainty to our estimates of net volumetric change. In contrast, our vertical datum uncertainty of $\pm$0.025 m would contribute $\pm$37,500 m^3 of volumetric uncertainty. Given the disparity of these numbers, we quantify our uncertainty in the analyses below solely under the framework of vertical datum uncertainty.

Our decision to effectively ignore spatially variable uncertainty is based on an analysis of our particular data sets and research interests and is not intended to be broadly transferable. In particular, our large area of analysis, our focus on total volumetric change and transport as opposed to finer spatial patterns, and the inconsistent GPS monumenting in our original surveys all conspire to make vertical datum uncertainties dominant in our study. Differing research questions, survey extents, and underlying accuracies will necessitate different means of assessing uncertainties.

3.4. Estimating Bed Material Transport From DoDs

When repeat surveys encompass the entirety of a basin, it is theoretically possible to estimate sediment fluxes down the length of the system. If there are no extrabasin sediment inputs and sediment leaves the

basin only through down-valley transport, the net volumetric lowering over the contributing area of a given point should be equal to the total volumetric transport past that point. Although simple in concept, actual application of this morphologic budgeting technique requires careful consideration of a host of factors to ensure that the results are unbiased and correctly interpreted. In our basin, simple conversions of volumetric change to transport volumes are complicated by uncertainties regarding bulk densities and the presence of glacial ice at the head of the basin.

The three surveys used in this study all extend upvalley of the glacial termini heading Tahoma Creek and so capture vertical changes over the entirety of the subaerial basin. Subglacially sourced sediments are not measurable using this method. Although this precludes us from estimating total sediment loads, previous research on the glacial streams around Mount Rainier has found that sediment loads at the glacial termini are composed largely of fine material traveling in suspension and that most of the coarse load is derived from entrainment of downstream sediments [*Fahnestock*, 1963; *Mills*, 1979]. As such, the subglacial and moraine sources should have distinct sediment distributions. An analysis of moraine sediments around Mount Rainier showed that material finer than 2 mm made up less than 35% of the deposits and D50 values ranged from 32 mm to 128 mm [*Mills*, 1978]. The percentage of fines was based on a sediment distribution truncated at 128 mm and so overstates the total percentage by an unknown amount. No samples were taken specifically from moraines of either the South Tahoma or Tahoma glaciers, but moraines around the mountain were quite similar and so provide a reasonable approximation for our study area. In comparison, subsurface sediment samples taken in the lower five VKs of Tahoma Creek during the summer of 2012 were, on average, composed of 18% material finer than 2 mm; D50 values ranged from 55 mm to 90 mm, with a mean of 71 mm. We take the similarities of the moraine and bed material as an indication that the former is the primary source of the latter and that subglacially sourced sediments are not contributing a significant volume of sediment residing in the bed. If such sediments did contribute significantly to the bed, we would expect to see a finer distribution.

Our inability to quantify subglacially sourced sediment fluxes means that our transport estimates do not reflect total loads. Nor do we capture pure bed load, as the morphological changes observed in moraine sediment and the downstream bed include a reasonable percentage of sediment that likely travel in suspension. As such, we call the fluxes quantified through this method bed material fluxes, which describe the fraction of the total load that forms the bed and lower banks of the channel.

If the bulk density of the moraine sediment is significantly different than the bulk density of the bed material, our estimates of transport based on volumetric change will contain some bias. Although we lack measurements of bulk densities in either setting, *Bunte and Abt* [2001] note that gravel-bedded channels have bulk densities that generally range between 1.7 and 2.6 Mg/m^3, with a mean of 2.1 Mg/m^3. Bulk densities taken from an active lateral moraine in Switzerland ranged between 0.84 and 2.34 Mg/m^3, with a mean of 1.7 Mg/m^3 [*Curry et al.*, 2009]. However, these bulk densities were measured from only a small volume, 0.1 m in diameter and 0.1 m in depth, and so constitute only the finer fraction of the material. Given the broad overlap over the range of bulk densities, and our lack of data with which to confidently quantify any true difference, we assume that the bulk densities of the two settings are essentially the same. If the mean values cited above are indeed reflective of our setting, this would make our transport estimates overly high by about 20%.

The presence of glacial ice in the upper basin of Tahoma Creek adds a source of uncertainty to our sediment transport estimates. Broadly, the entire upper basin holds a variable mixture of sediment and both active and stagnant ice, and the observed change in our DoDs is the product of both sediment mobilization and ice-mass loss. However, there are no data currently available that provide for even a rough estimate of the ratio of these two contributions across space. Therefore, we simply split this area into two zones: one in which ice-mass loss is assumed to be the dominant mode of change and one in which sediment mobilization is assumed to dominate. The areas of retreat of the active glacier between surveys were assigned to the former category; all points downstream of this zone were assigned to the latter. We attempted to estimate the potential magnitude of these errors to ensure that they do not overwhelm our estimates of transport.

From 2002 to 2008, there was roughly 300 m of glacial retreat, while negligible retreat was observed between 2008 and 2012 (Figure 4). For the earlier time period, we idealized the observed change within this zone of retreat as the sum of a constant ice-thickness loss and a variable depth of sediment incision. The histogram of change showed a roughly bell-shaped distribution. We assumed that the peak of this distribution

represented the constant ice-thickness loss. Change in excess of this thickness was attributed to sediment incision, and change less than this value was excluded from the analysis. This method produces an estimate of 5×10^5 m^3 of sediment incision. Given the roughness of this analysis, we elected not to include this volume in our estimates of sediment transport.

Photographs taken in 2012 show small outcrops of stagnant ice in the lower neoglacial sediment near VK 11, a clear indication that some percentage of the observed change within this zone represents ice-mass loss. We make use of observations made during a recent suite of debris flows to place some limits on the volume of ice-mass loss. *Scott et al.* [1995] noted ice making up to 10% of the total volume of debris flow deposits in 1986–1987. In contrast, *Walder and Driedger* [1994b] noted that the deposits of debris flows in the early 1990s contained no visible ice or frozen ground in their deposits, even though the flows clearly incised channels into stagnant ice. Though the depositional extent of ice provides a minimum estimate of the total volume of eroded ice, it provides some assurance that the true volume of eroded ice is not unreasonably large. We crudely estimate that source-area sediment may contain up to 30% ice, which would inflate our estimates of transport by the same amount.

Although these sources of error are not insignificant, they do not preclude us from making estimates of sediment transport with an accuracy that is at least comparable to those derived from sediment transport equations. We also note that the errors within the two zones operate in opposite directions and so are, to some degree, self-canceling.

3.5. Deriving a Sediment Rating Curve

For any location in the basin with coverage in all three surveys, the method above provides estimates of the total volumetric bed material transport over the two unique intervals between sequential surveys. These total bed material loads are the result of the integrated forces driving transport; for fluvial transport in the lower valley, this driving force is stream discharge. With estimates of two unique bed material loads and estimates of the hydrology driving that transport, it is possible to back out a simple two-parameter sediment transport rating curve. We choose to use a rating curve of the form $Q_s = a(Q - Q_c)^b$, a common form for simple bed load formulas [*Meyer-Peter and Müller*, 1948; *Rickenmann*, 2001]. In this formula, Q_s is the total daily load (kg/day), Q is the daily mean flow (m^3/s), and Q_c is the critical discharge below which it is presumed no transport occurs. If we impose a critical discharge, Q_c, it is then possible to numerically solve for the unique values of a and b that satisfy the paired equations

$$\int_{t_1}^{t_2} a(Q - Q_c)^b = \mathrm{AL}_{02-08} \tag{4}$$

$$\int_{t_2}^{t_3} a(Q - Q_c)^b = \mathrm{AL}_{08-12}, \tag{5}$$

where AL indicates the accumulated load over the noted period as estimated from lidar. The derived values of a and b then define the functional relationship between discharge and bed material transport at a given location in Tahoma Creek, and the rating curve as a whole provides a temporally continuous estimate of sediment transport rates with daily resolution.

3.6. Estimating Streamflow

Deriving a rating curve in the manner described above requires continuous estimates of discharge over the entire period of observations (2002–2012). With the exception of a brief period of record obtained during the summer of 2012, such discharge observations are not available for Tahoma Creek, and so had to be estimated through analysis of several nearby gages. The process of estimating discharge on Tahoma Creek was not trivial and so is described in some detail.

The stage of Tahoma Creek was measured using a pressure transducer mounted on the Tahoma Creek Bridge, providing measurements every 15 min from 14 June to 24 August 2012. Weekly discharge measurements were used to construct a discharge rating curve, although the highly mobile bed made this a nontrivial effort. This record was then used as a target with which to assess the accuracy of discharge estimates derived from analysis of Nisqually River flow at National, where the USGS has had a gage since 1943, and flow at Longmire, where a National Park Service gage has been in operation since October of 2009 (Figure 1 for both sites). Although the Longmire records are limited, they provide a few years worth of data

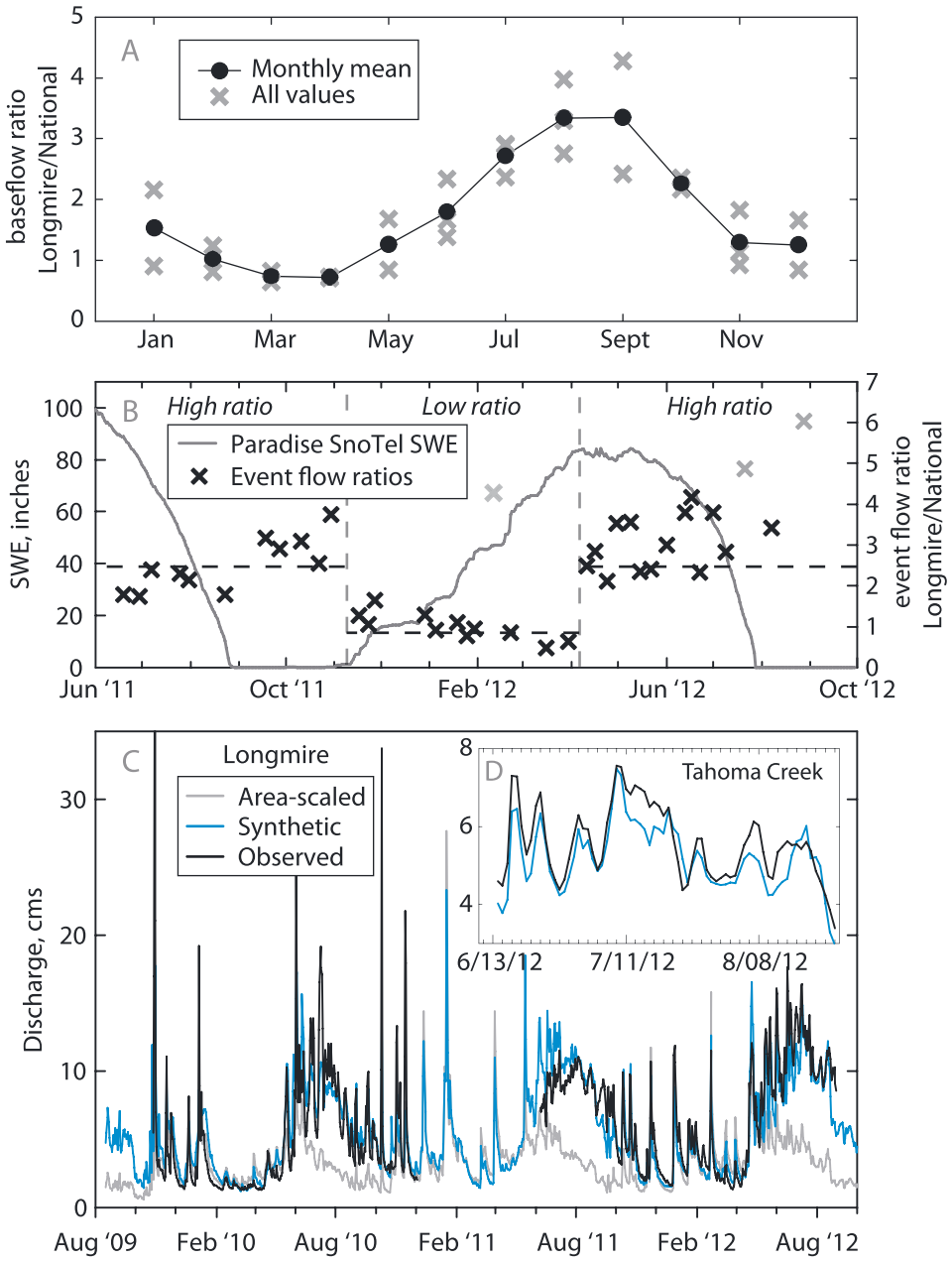

Figure 6. Various components of the synthetic hydrograph process. (a) Monthly mean, unit area base flow ($m^3/s/km^2$) ratios for Longmire/National, showing all individual months and means for each month. (b) Unit area event flow ($m^3/s/km^2$) ratio for Longmire/National, shown in relation to snow water equivalent (SWE) as measured at the Paradise SnoTel station (see Figure 1 for location). Accumulation season onset and peak SWE are shown as vertical grey dashed lines dividing the record into periods of high and low ratios. The means for the two period types are indicated by black dashed lines. Outliers, excluded in the estimation of the means, are indicated in grey. Comparisons of the derived synthetic hydrographs with the observed flow is shown for (c) Longmire and (d) Tahoma Creek. In Figure 6c, flows predicted for Longmire produced by scaling the discharge at National by drainage area ratios are also shown to highlight the improved performance of the synthetic method during the melt season.

with which to develop a relationship between the mixed lowland-glacial flows measured at National and the glacially dominated flows measured at Longmire. We then assumed that flows on the Nisqually at Longmire were highly correlated with flows on Tahoma Creek at the bridge, given their similar basin areas, glacial extents, elevations, and their close spatial proximity. The Longmire-National relationship was thus rescaled to the drainage area of Tahoma Creek and compared against our limited period observations.

Flows measured at Longmire and National did not scale simply, reflecting the difference in relative importance of high-elevation snow and ice. To develop a relationship between these two regimes, all flow records were first separated into base flow and event flow components using a local-minimum method [*Pettyjohn and Henning*, 1979]. Because the rating curve used at Longmire for records before December 2010 was poorly defined at high flows and produced what we judged to be unrealistically large high flow events, we removed the event flow component of these records from the analysis, leaving us with Longmire base flow estimates from October 2009 onward but with event flow only after December 2010. Base flow and event flow records were normalized by contributing area ($m^3/s/km^2$) and then used to examine the temporal variations in the correlation between flows at Longmire and National.

Monthly mean base flow ratios (Longmire/National) reflect the influence of summer melt from glacial ice and snow, with Longmire having a relatively higher base flow during summer and early fall and a relatively lower base flow during the winter. This ratio varied smoothly over the course of the year (Figure 6a). In contrast, peak event flow ratios (based only on the highest flow for a given event) showed a bimodal distribution (Figure 6b). Comparisons of the distribution of this ratio to snow depth records at the Paradise Snotel site (Figure 1) shows that low ratios occur between the onset of the accumulation season and the occurrence of peak snow water equivalent (SWE), when precipitation at higher elevations falls primarily as snow, whereas high ratios occur during the snowmelt and summer seasons. Although there appears to be a linear trend of increasing event flow ratio with increasing time since peak SWE, we lack sufficient data to parameterize this relationship.

Flow at Longmire for the period between 1943 and 2012 was estimated using the equation

$$Q_{\mathrm{lm}} = A_{\mathrm{lm}}[\mathrm{BFR}(Q_{\mathrm{n-base}}/A_{\mathrm{n}}) + \mathrm{EFR}(Q_{\mathrm{n-event}}/A_{\mathrm{n}})], \tag{6}$$

where the subscript lm refers flow at Longmire, the subscript n refers to flow at National, and A refers to the drainage areas of the basins. BFR and EFR refer, respectively, to the base flow and event flow ratios observed (Figures 6a and 6b), with the former being a continuous function of the day of year and the latter being a bimodal function based on observed snow depths at the Paradise Snotel site. For years before 1980, for which Snotel data were not available, the mean 1980–2012 onset date of the snow accumulation period and date of peak SWE were used to determine whether the high or low event flow ratio was appropriate. The results of this process provide improved agreement for flows during the melt season, when compared against simple area-scaling flow estimates (Figure 6c).

These estimated flows where then rescaled to the drainage area of Tahoma Creek. The resulting synthetic discharge showed good relative agreement with our observations but was consistently higher than the measured discharge by ~50%. A simple scalar was multiplied through the relationship to correct this offset, producing our final estimated flows (Figure 6d). The root-mean-square error of the fit was 0.5 m^3/s, roughly corresponding to a ±10% error over the range of flows observed. To determine if our estimates for peak flows were reasonable, we compared our synthetic estimate of the 2006 flood to photos taken before, during, and immediately after the event, allowing us to roughly estimate flow depths. Using the bridge's width of 20 m and assuming a flow velocity of 2–3 m/s, our predicted flow of 68 m^3/s gives a depth of about 2 m, in rough agreement with the flow depth inferred from the photos.

The synthetic discharge records we created are valid for locations immediately around the Tahoma Creek Bridge. However, drainage area at VK 4.5 is 70% of that at the bridge, and no major tributaries enter the stream between VKs 0 and 4.5. Given this, we assume that the synthetic records are sufficiently accurate to be used in our rating curve analysis over this reach. Although applying an area-scaled correction to the synthetic discharge records is straightforward, we found that applying such linear changes to the entire hydrologic record only modifies the coefficient of our rating curve and not the exponent. Therefore, an area-scaling correction only impacts the apparent efficiency of transport and not the functional form of the discharge-transport relationship. This result can be understood by considering that multiplying the entire hydrologic record by a single value is also how flow records would be transformed from cubic feet per second to cubic meters per second. Such a change of units impacts only the coefficient of a rating curve but would not change the physical scaling of transport as a function of discharge, as described by the exponent.

Above VK 4.5, flow is split between the main thread of Tahoma Creek and Fish Creek, and so our discharge estimates are clearly in error. Although our method will produce a numerical result upstream of this point,

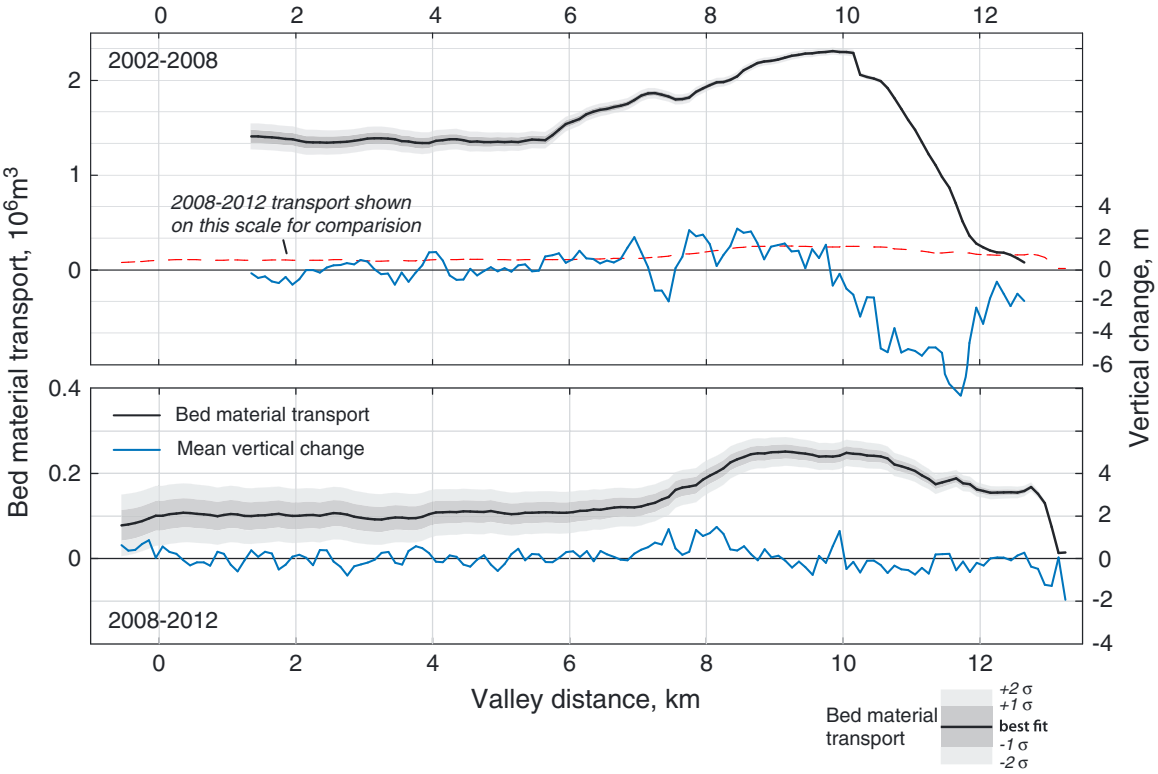

Figure 7. Mean vertical change and estimated bed material transport as derived from lidar differencing. Vertical scales for the two time periods are different. The red dashed line in the top plot shows the 2008–2012 transport rates plotted on the same vertical scale as the 2002–2008 transport rates, allowing for a more direct comparison. Light and dark grey shading represents transport estimates for vertical datum offsets of ±5 cm (2σ) and ±2.5 cm (1σ), respectively.

its physical interpretation becomes less clear, both because the discharge is clearly unrealistic and because much of the transport likely occurred by debris flow events. We present numerical results above VK 4.5 to illustrate the apparent stability of the method, but we do not interpret or extrapolate from those values.

3.7. Critical Discharge

Since two time periods of analysis give us only two accumulated load equations (equations (4) and (5)), we are able to solve for only two free parameters in our rating curve. Because there are three free parameters (a, b, and Q_c), we must fix one before solving for the remaining two. We chose to fix Q_c, solving for a and b. We use two plausible values of Q_c: 0 m^3/s, representing unthresholded transport described by a pure power law, and 5.5 m^3/s, a value based on the numerous shifts observed in the stage-discharge relationship developed over the summer of 2012. These shifts occurred after flows at or above this discharge and represent the restructuring of the bed. Thus, they are a rough guide to mobility. Using cross sections taken during discharge measurements, slopes measured from lidar, and sediment characteristics from extensive sediment sampling along the lower 5 km of the channel, we estimate that a flow of 5.5 m^3/s is equivalent to a critical shear stress of 0.07–0.09, in good agreement with several recently developed formulas for critical shear stress; for the 0.03 slope at our site, *Mueller et al.* [2005] predicts a critical shear stress of 0.086, while *Lamb et al.* [2008] predict a critical shear stress of 0.062.

3.8. Uncertainty Quantification

To estimate the uncertainty of our estimates of a and b, we performed a 500-run Monte Carlo analysis. For each run, two random vertical offsets (representing vertical datum uncertainty) were taken from a normal distribution ($\mu = 0$, $\sigma = 0.025$) and added independently to the two DoDs, after which new bed material loads were estimated. The hydrology for both time periods was multiplied by a single random normally distributed value ($\mu = 0$, $\sigma = 0.2$). These quantities were then used to calculate new values of a and b and the distribution of these values taken to represent our uncertainty. As this accounts only for uncertainties in our vertical datum and our synthetic hydrology, and not the interpretation errors discussed in section 3.4, it is a low estimate of the total uncertainty. Because we quantify uncertainty solely under the framework

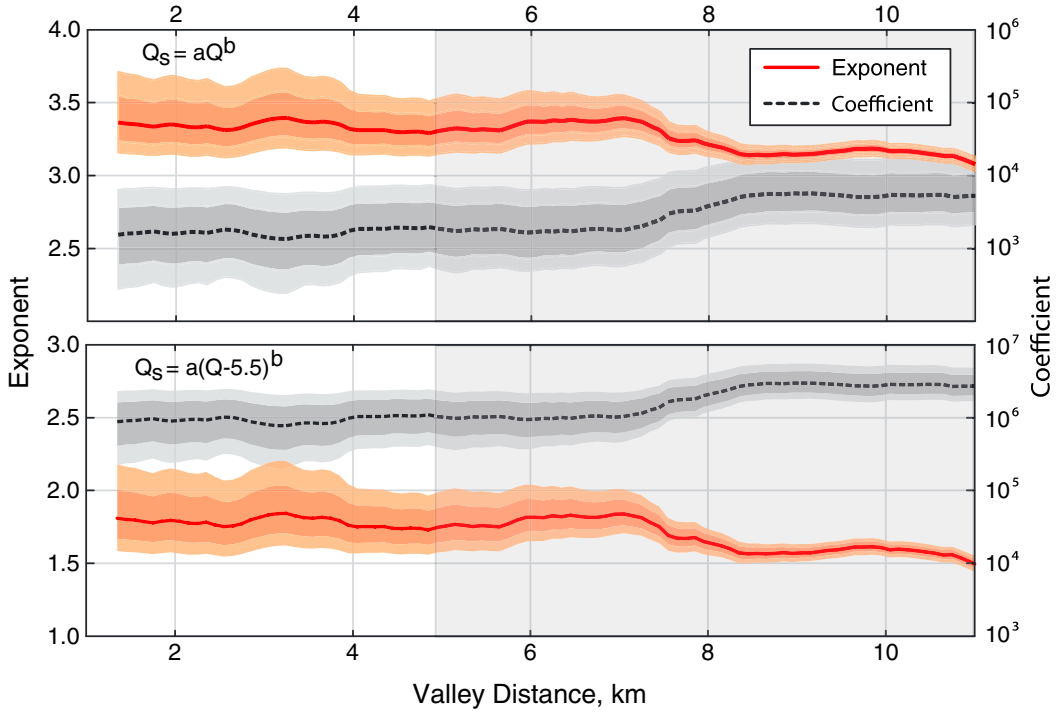

Figure 8. Rating curve coefficients and exponents as derived from lidar analysis using the two indicated power law relations. As discussed in the text, our results are likely valid only downstream of VK 4.5. Although the results upstream of VK 4.5 appear well behaved, their physical meaning is not obvious. Light and dark shading around result lines represent one and two standard deviations of uncertainty, as calculated from Monte Carlo analysis.

of vertical datum uncertainty, which increases in volumetric magnitude as a linear function of contributing area, our uncertainty in both transport estimates and values of *a* and *b* increase downstream.

4. Results—Analysis of Repeat Lidar

4.1. Description of Change and Transport, 2002–2008

The 2002–2008 time period is dominated by the extensive work of an extremely large flood in November of 2006. Above VK 10, 2.3×10^6 m^3 of unconsolidated glacial sediment were mobilized (Figures 4 and 7). It is likely that this material was mobilized by debris flows, given the prevalence of such events in Tahoma Creek. Of this total volume, 1×10^6 m^3 was deposited between VKs 4 and 9, and the remaining 1.3×10^6 m^3, along with 50,000 m^3 entrained from downstream reaches, was transported beyond the extent of the 2002 survey (Figure 7). Below VK 4, the river incised slightly, with a net lowering of 0.07 m. Two localized zones of aggradation seen at VKs 3.2 and 4 are correlated with a marked decrease in channel slope and significant logjams, respectively. Between VKs 3.5 and 8, repeated debris flows and the intensity of the 2006 flood caused the main thread of Tahoma Creek to wander markedly and resulted in a significant avulsion between VKs 3.5 and 4.5, with the channel abandoning its eastern course to flow through what had previously been forested area along the western margin of the valley.

4.2. Description of Change and Transport, 2008–2012

Significantly less transport occurred at all points in the basin between 2008 and 2012. Above VK 10, 250,000 m^3 of material was mobilized, predominately sourced in sediments mantling a steep bedrock step just below the 2012 glacier terminus (Figure 4). Lateral moraines showed significant downslope motion of material, but the majority was deposited directly at the bases of the slopes, with only a modest volume mobilized downstream. About 150,000 m^3 of material was deposited between VKs 8.5 and 7. Below VK 7, calculated transport volumes were about 100,000 m^3 with little downstream variation. Although the channel in this lower area was reworked laterally, it remained vertically stable over most of its length. The only major exception occurred downstream of the Tahoma Creek Bridge (VK 0), where 25,000 m^3 of material was deposited in the fan at the stream's confluence with the Nisqually River.

In both time periods, roughly half of the material mobilized from the upper basin above VK 10 was deposited between VKs 10 and 6, while the remainder continued downstream to exit the system. Although significant volumes of sediment were transported through the reaches below VK 5, they remained vertically stable, with no apparent aggradational or incisional trend observed over the 11 year period we analyzed.

4.3. Rating Curve Results

Over the physically meaningful reaches between VKs 1.3 and 4.5, the coefficients and exponents of both our unthresholded and thresholded rating curves show no trends or variability in the downstream direction (Figure 8). Exponents were approximately 3.3 ± 0.2 and 1.8 ± 0.2 for the unthresholded and thresholded forms, respectively. Coefficients were 1700 ± 1600 and $9.4 \times 10^5 \pm 5.8 \times 10^5$ for the unthresholded and thresholded forms, respectively.

At present, we do not have any quantitative data to suggest which of the two forms of our rating curve better matches physical processes in Tahoma Creek. By design, both rating curves predict exactly the observed total loads between 2002–2008 and 2008–2012. Both give similar results when used to estimate transport loads over the period of our synthetic hydrology (1943–2012), $68{,}000 \pm 15{,}000\ m^3/yr$ for the thresholded form compared to $47{,}000 \pm 9000\ m^3/yr$ for the unthresholded form. Both equations predict similar transport volumes for the 2006 event. The thresholded form eliminates the need for a single power law to explain transport across flows ranging from 1 to $68\ m^3/s$ and so may be more accurately tuned over the higher flows that transport the majority of sediment. However, the use of a threshold adds curvature to the discharge-transport relationship in log-log space. This curvature complicates comparisons between our rating curve and modern transport equations, which generally do not contain similar thresholds. As such, we present annual bed material loads calculated using our thresholded rating curve but use the unthresholded form to aid in comparisons with rating curves derived from both bed load measurements and transport equations.

4.4. Assessment of Results

To assess whether our estimates of bed material transport and the derived rating curves are reasonable, we compare our results to prior estimates of sediment transport, focusing on research around Mount Rainier.

4.4.1. Additional Lidar-Derived Bed Material Estimates

The most direct comparison of our results comes from lidar-derived bed material transport estimates from the Kautz, Carbon, and Nisqually basins, all proglacial catchments around Mount Rainier. As all of these basins are covered by 2008 and 2012 aerial lidar surveys, we used the same methodology outlined for Tahoma Creek to produce estimates of the bed material transport over this period. At locations with drainage areas similar to that of Tahoma Creek, the Carbon River transported $1.2 \times 10^5\ m^3$, while the Nisqually River transported $0.8 \times 10^5\ m^3$. The uncertainties in these values are comparable to those of transport in Tahoma Creek over this same period (±75%, Figure 7), but they are very similar to the best fit values of $\sim 1 \times 10^5\ m^3$ estimated for Tahoma Creek. Kautz Creek, which is armored with coarse sediment from 2005 and 2006 debris flows, showed no detectable transport.

4.4.2. Mount Rainier Bed Load Measurements

A limited number of sediment transport measurements taken on rivers draining Mount Rainier provide some means of directly assessing our sediment rating curve. Compiled measurements from multiple streams [*Czuba et al.*, 2012a] are fit with a power law, giving an exponent of 2.36 and a coefficient of 5.7. Extracting data from just the White River, the most abundant from a single source, gives an exponent of 3.16 and a coefficient of 0.2. Comparing these number with our results from the unthresholded rating curve, our coefficient is significantly higher, but our exponent is similar to these measurements. We note that these measurements were taken during flows that range from only 4% to 12% of the mean annual flood at the sampling sites and so represent only the low-flow component of their rating curve. As such, they may not be entirely comparable to our rating curve estimates, which extend up to the flood of record for our site.

4.4.3. Alder Lake Sedimentation

Alder Lake, a reservoir on the Nisqually River in operation since 1945, provides a means for estimating total loads for the whole of the upper Nisqually basin, of which Tahoma Creek represents 10% as measured by area. Surveys of the delta completed in 1945, 1956, 1985, and 2011 provide estimates of total sediment deposition over multiple time periods [*Czuba et al.*, 2012b]. To compare these results with our estimates of bed material transport in Tahoma Creek, we must estimate what percentage of the delta deposition documented in Alder Lake consists of coarse material. In the absence of any sediment samples of these delta deposits, we assume this could reasonably range from 20% to 40% [*Pratt-Sitaula et al.*, 2007; *Wallick et al.*,

Table 2. Data Pertaining to Aerial Lidar Data Used in This Analysis[a]

Period	Alder Lake Deposition, Total (1000 m^3/yr)	Alder Lake Deposition, Bed Material (1000 m^3/yr)[b]	Tahoma Creek Bed Material Transport (1000 m^3/yr)[c]	Tahoma Creek as Percentage of Alder Lake[d]
1956–1985	430 ± 86	130 ± 70	40 ± 12	31% (13%–74%)
1985–2011	770 ± 154	230 ± 120	87 ± 14	37% (19%–81%)
1956–2011	590 ± 118	170 ± 90	62 ± 13	35% (17%–78%)

[a]Information regarding the larger survey which our 2002 data are a subset of is available in *Harding* [2004]. The 2008 and 2012 survey data are taken from *Watershed Sciences* [2009] and *NCALM* [2012], respectively.
[b]Values assume that 30% of total deposition is composed of bed material, with uncertainty encompassing a range from 20% to 40%.
[c]Estimated using thresholded power law relation at VK 1.3.
[d]Values in parentheses represent range of values based on uncertainties presented.

2010]. These relatively high values reflect the steep nature of the contributing streams, in which coarse material transported as bed load is likely to constitute a large percentage of the total load, and the fact that the finest fraction of sediments may be transported beyond the surveyed extents of the delta. Uncertainties in the raw delta surveys were dependent upon which interval was used but were always less than $\pm$20%, and so we elect to use this value as a conservative upper bound. Because sedimentation from 1945 to 1956 is dominated by input from massive Kautz Creek debris flows in 1947, we exclude this period from comparison.

We compared our estimates of bed material deposition in Alder Lake against Tahoma Creek bed material transport at the downstreammost cross section for which a rating curve was developed, at VK 1.3. Using our synthetic hydrology extending back to 1943, we calculated total transport through this cross section for the same time intervals of the delta surveys. Uncertainties in the Tahoma Creek transport volumes are taken from the Monte Carlo analysis described in section 3.8.

Using best fit transport values and assuming that 30% of the Alder Lake delta is composed of bed material, our estimates of transport in Tahoma Creek represent about 35% of the bed material deposition in the delta (Table 2). Accounting for uncertainty in both our transport estimates and our estimates of bed material deposition in Alder Lake, this value could range from 15% to 80%.

4.5. Summary

Although none of the assessments above provide unequivocal evidence that our methodology produced accurate estimates of bed material transport in Tahoma Creek, the coherency of the results is heartening. We find the Alder Lake comparisons particularly persuasive; that Tahoma Creek, 10% of the Alder Lake drainage by area, would contribute 35% of the coarse sediment is reasonable, given the abundant glacial sediments present in the basin.

The reasonableness of our results can be further demonstrated by constructing a rough sediment budget for the Nisqually River above Alder Lake. Under the simple assumption that the three glacially headed basins of the Alder Lake drainage (Tahoma Creek, Kautz Creek, and the upper Nisqually) all produce roughly equal sediment loads, these basins would provide the full depositional volume seen in the Alder Lake delta. This assumption of equal transport has some support from estimates of 2008–2012 transport volumes for the upper Nisqually and was likely more valid for Kautz Creek before the 2006 floods. Sediment delivery rates for unglaciated terrain around Mount Rainier have been estimated at 70 ± 25 $m^3/km^2/yr$, based on additional repeat delta surveys in a lower arm of Alder Lake [*Czuba et al.*, 2012b]. Presuming that this sediment delivery rate is applicable outside of subglacial areas and the immediate glacial forefield, this sediment production rate would translate into $40{,}000 \pm 14{,}000$ m^3/yr over the 580 km^2 of unglaciated contributing area to the Alder Lake delta or between 4% and 8% of the observed sediment accumulation rate. This low value lends support to the idea that the glacially headed basins provide the overwhelming majority of sediment seen in Alder Lake. Although this crude sediment budget is speculative, the results are coherent and plausible.

Finally, over the range of uncertainties we present, our estimates of transport in Tahoma Creek never exceed 100% of estimated deposition in Alder Lake, leaving our results physically possible, if not always probable. We consider this level of agreement with observations a success in the context of the order-of-magnitude uncertainties that are commonly present in sediment transport estimates. Thus, while acknowledging that our results are subject to uncertainty, we assert that they are sufficiently accurate to act as a benchmark

against which to test the skill of previously developed bed load transport equations. Our estimates of accumulated transport volumes, based directly on conservation of mass, are likely more robust benchmarks than our derived rating curve. Similar methods have been used in previous assessments of bed load transport predictions [*Chiari and Rickenmann*, 2011].

5. Evaluating Bed Load Transport Equations

Many prior studies have documented the low skill of bed load transport equations in steep settings, which often predict transport rates orders of magnitude higher than those observed [*Bathurst*, 2007; *Yager et al.*, 2007; *Chiari et al.*, 2010; *Nitsche et al.*, 2011]. However, given the investments of time and money that are required to obtain even a few bed load transport measurements, these equations are often the only available option for predictions of bed load transport rates. Such rates are a necessary component of river engineering projects, hazard predictions, and in developing an understanding of both geomorphic and ecologic processes in mountainous terrain. Given this need, we assessed whether several modern transport equations were able to reproduce our lidar-derived transport estimates. We further tested if these equations were improved by the incorporation of several modifications that have recently been proposed for the application of transport equations in steep settings.

5.1. Methods—Bed Load Equations

We chose to test three equations—surface-based *Parker* [1990], *Wilcock and Crowe* [2003], and *Recking* [2010]. Although a more recent formulation of Recking's equation is presented in *Recking* [2013], we elected to use his original formulation as it allows for the direct manipulation of the critical shear stress. In addition to the original forms of the transport equations, we also employed two modifications that aim to reduce the tendency to overpredict transport. In one case, we calculated transport for the three equations using a reduced slope, accounting for energy losses due to large roughness elements. We operationalize this by combining equations (31) and (32) in *Rickenmann and Recking* [2011] to get

$$S_0 = p^e S^{1-ez}, \tag{7}$$

where S is the original slope, S_0 is the reduced slope, and p, z, and e are empirical constants. We set $p = 0.07$, $z = 0.47$, and $e = 1.2$, values suggested in their paper and which provide a reasonable fit to their data as well as to data compiled by *Palt* [2001] and *Chiari et al.* [2010]. In the second case, we replace the originally specified critical shear stress in each of the equations with the slope-dependent formula of *Mueller et al.* [2005]

$$\tau_{*c} = 0.021 + 2.18S \tag{8}$$

derived from an extensive bed load sampling campaign undertaken in Idaho streams.

Inputs to these various formula include topography, sediment-size distributions, and estimates of hydraulic parameters. Cross sections and channel slopes for Tahoma Creek were obtained from the 2008 lidar. To estimate grain-size distributions, 25 surface and 6 subsurface samples were taken along the lower 5 km of the channel. Surface samples consisted of 200-clast Wolman pebble counts, recorded at half-phi intervals down to 2 mm. For subsurface samples, the surface layer was removed, and 300–500 kg of subsurface sediment was collected. Particles coarser than 32 mm were sorted and weighed in the field, whereas a 5 kg sample of the <32 mm material was retained and later sieved down to 0.35 mm. There were no significant downstream trends in sediment distributions over the lower 5 km, and armoring ratios were indistinguishable from 1. Therefore, we combined all surface and subsurface measurements into a single distribution that was used in all locations. D16, D50, and D84 values for this distributions were 1.4 mm, 72 mm, and 205 mm, respectively, with 18% of the material finer than 2 mm. For the Parker equation, the distribution was truncated at 2 mm, as per the original paper. Flow depths and velocities at a cross section were estimated using *Ferguson*'s [2007] flow-resistance equation, which provided good agreement with stage-discharge relations observed at the Tahoma Creek Bridge. Because lateral variability in shear stress along a cross section has been shown to be important for accurate transport estimates [*Ferguson*, 2003], we subdivided our cross sections into 1–10 m sections, with the length being a function of the terrain complexity, and calculated flow depths, shear stresses, and transport rates for each subsection individually. The subsections were then summed to give total transport at the cross section. We used this process to calculate sediment rating curves for flows

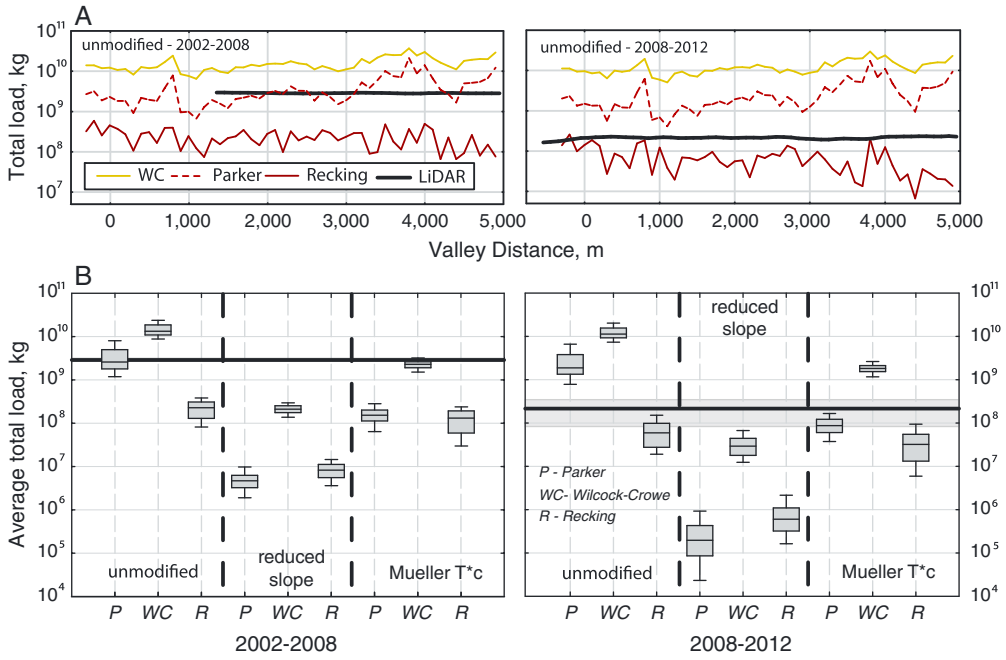

Figure 9. Sediment transport predictions from transport equations, compared against lidar-derived values. (a) Downstream trends for unmodified equations of *Parker* [1990] (P), *Wilcock and Crowe* [2003] (WC), and *Recking* [2010] (R). The similarity between predicted transport over the two time periods is a result of large volumes of transport predicted during low flows, such that total transport volumes are relatively insensitive to hydrology. (B) Box plots of transport predictions for all cross sections for a given equation and its modifications. lidar-derived values are shown as black lines, with grey shading indicating ±5 cm of vertical uncertainty. For the 2002–2008 period, this uncertainty was on the scale of the line thickness and so is not visible.

ranging from 0.3 m^3/s to 80 m^3/s every 100 m down the lower 5 km of channel, for a total of 50 locations. These computed rating curves, in combination with the synthetic flow records described in section 3.6, were then used to predict total bed loads over the time steps for which lidar-derived estimates exist. This process was repeated for all three equations noted above, using three forms (unmodified, reduced slope, and Mueller's τ_{*c}), for a total of nine results per time period.

5.2. Results—Bed Load Equations

The transport equations were evaluated based on how well they reproduced both the total sediment volumes and the form of the sediment rating curve we derived from lidar. All equations and their variants did a reasonable job of reproducing the observed consistency in downstream transport volumes, albeit with significant noise (Figure 9a). Given the lack of downstream trends in transport, we summarized the transport prediction results using box and whisker plots (Figure 9b). Although several of the equations predict total transport volumes similar to those estimated from lidar for one time period or the other, no single equation performed well in both periods. Accumulated transport volumes vary only slightly between the two periods for any given equation, despite the disparity in the hydrology of the two periods (namely, the occurrence of the 2006 flood). The lack of sensitivity is a function of the high volumes of transport these equations predict during low flow, such that total transport volumes are relatively insensitive to the flood hydrology of a given period (Figure 10). For example, the unmodified Parker and Wilcock-Crowe equations predict 60% and 80%, respectively, of all 2002–2012 transport to occur during flows below 5.5 m^3/s, our estimated critical discharge. In contrast, the Parker and Wilcock-Crowe equations predict modest transport volumes over the course of the 2006 flood, with the event constituting only 10% and 2% of respective accumulated transport volumes. This is in contrast to our lidar-derived estimates, in which 0%–10% of all transport was estimated to occur below 5.5 m^3/s and the 2006 flood constituted 65%–80% of total estimated transport. Direct comparison of the rating curves (Figure 11) show the root of this discrepancy. At low to moderate flows, the Parker and Wilcock-Crowe curves predict much higher transport rates than the lidar curves. However, there is a crossover in the 10–20 m^3/s range, above which our lidar rating curves predict transport rates at least

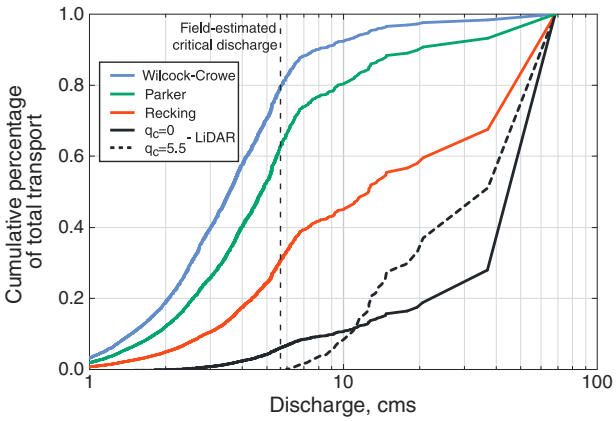

Figure 10. Cumulative bed material transport for the 2002–2012 period as a function of discharge, expressed as a percentage of the total transport predicted.

an order of magnitude higher than any of the equations. Both in terms of low-flow transport volumes and transport during the 2006 flood, the Recking equation more closely matched our lidar baseline than either of its competitors, though still predicted higher transport rates at low flows and lower transport rates at lower flows.

Transport rates estimated using a reduced slope resulted in underprediction of transport volumes for all three equations over both periods, significantly so for both the Parker and Recking equations (Figure 9b). Use of Mueller's τ_{*c} leads to similar underpredictions over the 2002–2008 time period with the exception of the Wilcock-Crowe equation. However, given our discussion above and the fact that the equation did not perform well over the 2008–2012 time period, the apparent success is likely spurious. Both the Mueller-modified Parker and Recking equations produced loads close to those observed over the 2008–2012 time period, and the ratings curves for these equations are not entirely dissimilar from our lidar-derived curves over the range of flows that occurred over this later period (2–15 m^3/s) (Figure 11).

6. Discussion

Based on the assessments we present in section 4.4, we assert that the morphologic budgeting technique we have used here, as well as the derived rating curves, provide reasonably accurate estimates of bed material transport in Tahoma Creek. Presuming that further testing bears out this apparent success, these methods could provide estimates of transport rates in steep streams.

Several aspects of Tahoma Creek make it particularly amenable to these techniques. The basin is very active, with clearly defined and largely vegetation-free zones of transport. Only a small percentage of the active channel is submerged during the later summer months, making it a good candidate for analysis using conventional airborne lidar. Our surveys captured the entire bed material source area, avoiding complications associated with compensatory scour and fill [*Lindsay and Ashmore*, 2002]. The source area, composed of rapidly incising lateral moraines, lowered many meters between surveys, making detection straightforward and relatively robust. Our ability to back out a sediment rating curve from our observations of volumetric transport was improved by the immense disparity in the hydrology and associated sediment transport during the two time periods analyzed. Given that the rating curve analysis boils down to a best fit procedure in which, in essence, a line is fit to two fuzzy points, the greater the separation between these points, the less uncertainty in the results.

Even with these benefits, our estimates of the 2008–2012 transport involve a 2σ uncertainty of nearly $\pm$90% (Figure 7). Such uncertainty suggests that applying these same morphologic budgeting methods in vegetated or relatively inactive areas may be difficult. These methods also include significant investments, both financially and in terms of time, as enough landscape change must accumulate such that it can be meaningfully detected by the chosen survey method. The 10 years of change documented here illustrate that, even in active settings, sufficiently detectable change may take time.

Improvements in the accuracy of current survey methods, or the development of new methods that allow for accurate surveying of vegetated or submerged topography, would both improve the accuracy of morphologic budgeting techniques and broaden the range of areas over which they can be applied [e.g., *Williams et al.*, 2013; *Fonstad et al.*, 2013]. With that in mind, we note that the methodologies we use in this paper are not specific to either aerial lidar or assessments of bed material transport. In particular, the method we used to derive a sediment rating curve from our observations of total transport could be applied equally well in any situation where sediment loads were known for at least two time periods, along with

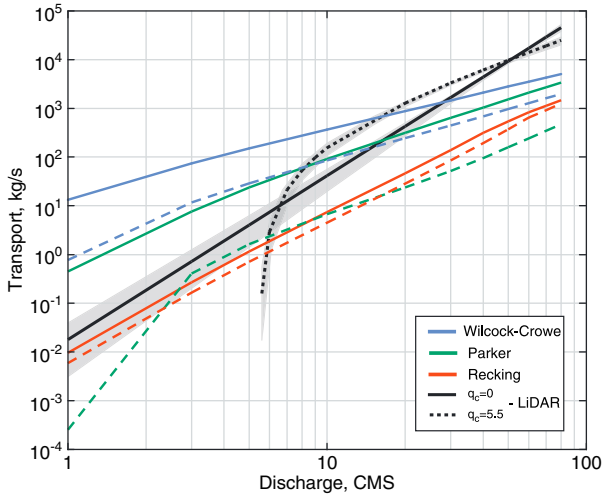

Figure 11. Predicted bed load transport rating curves at VK 1.3, as compared to lidar-derived bed material curves. Solid lines represent unmodified equations, while dashed lines represent the use of Mueller's τ_{*c}. Rating curves using the shear-partitioning method plotted very low and so were omitted for clarity. Grey shading indicates 2σ uncertainty range for our lidar-derived results, as quantified through our Monte Carlo analysis.

records of discharge for the intervening period. Repeat reservoir surveys are the most obvious target, especially given the increasing ease and accuracy of such surveys.

As an example, the Alder Lake delta surveys used to assess our results provided total accumulations from 1956–1985 and 1985–2011, while the USGS gage at National provides daily discharge records just upstream of the delta back to 1943. Using the same (unthresholded) power law form we used in Tahoma Creek, our rating curve method estimated an exponent of 3.4 and a coefficient of 1.4×10^{-8} for total sediment transport in the Nisqually just above Alder Lake. These values do not seem particularly unreasonable, and the similarity of the exponent to what we estimated in Tahoma Creek is interesting though quite plausibly coincidence. However, using these values to predict total sediment transport over the 1945–1956 time period produces a transport value that is nearly four times lower than what was observed. This discrepancy is likely the result of the accelerated transport rate associated with the Kautz Creek debris flows of 1947 and points to an inherent assumption in this method, namely, that the discharge-transport relationship is unchanging over the period of consideration.

The assumption of stationarity is unlikely to be valid over short time scales of seconds to days; observations in both natural systems and flume experiments have demonstrated the ubiquitous occurrence of pulses and waves in coarse sediment transport, with order-of-magnitude fluctuations in transport rates even under steady flow [*Iseya and Ikeda*, 1987; *Kuhnle and Southard*, 1988; *Gomez et al.*, 1989; *Venditti et al.*, 2010; *Recking*, 2013]. Because our rating curve inherently averages out these fluctuations, this method is unlikely to be particularly useful for exploring the fine-scale, transient processes that ultimately control instantaneous transport rates. However, *Recking et al.* [2012] noted that sediment transport predictions generally increase in skill as the time scale over which they are assessed increases. This suggests that discharge-transport relationships may often be stationary, such that observed fluctuations move around a stable mean equilibrium value. Indeed, such an assumption underlies many estimates of sediment transport, where individual observations encompassing immense scatter are approximated by a single best fit curve [e.g., *Recking*, 2013, Figure 2]. In situations where the assumption of stationarity is valid, the averaging that occurs in our method may actually be considered a benefit, smoothing over a range of temporal and spatial variability to arrive more directly at the equilibrium transport relationship. More problematic is the potential for stochastic events or climate shifts, operating over time scales similar to or longer than the period of observation, which can significantly alter the discharge-transport relationship. The 1947 Kautz Creek debris flows are one potential example of this issue. In Tahoma Creek, the 2006 flood may have been such an event, altering the discharge-transport relationship either through passage of hyperconcentrated flows following debris flows or by changing the threshold of mobility. Our data do not provide any means of assessing whether this occurred.

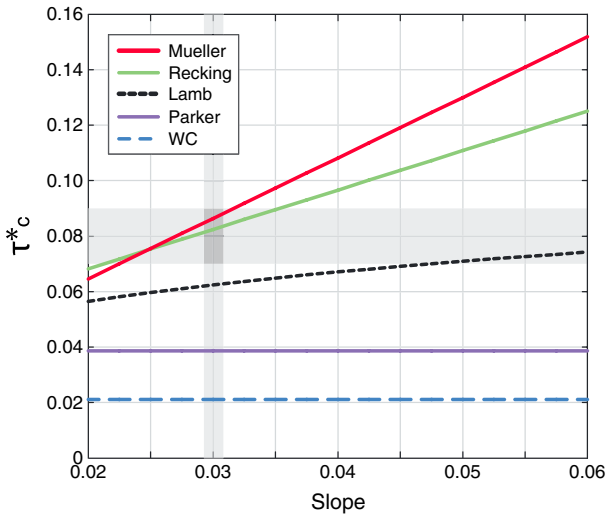

Figure 12. Comparison of predicted critical shear stress values as a function of slope from a variety of equations to estimated field values for Tahoma Creek. Grey bars indicate the range of slopes and critical shear values computed near the Tahoma Creek Bridge. Field values for critical shear were estimated by observing what stage of flows produced shifts in the hydrologic rating curve.

While acknowledging the potential for low-frequency extreme events to complicate our rating curve methodology, the method should broadly be the most accurate for transport rates at high flows. Larger events transport larger volumes of sediment and so produce larger and more distinct changes in the landscape, the quantity we ultimately measure. This can be seen in our lidar-derived rating curves seen in Figure 11, where the difference between the curves, as well as the uncertainty of those curves, is least for flows between 40 and 70 m^3/s, corresponding to the flows over the 2006 flood. The potential to constrain transport rates for these high flows makes this method a strong complement to more direct transport measurement methods that generally struggle in such events.

Assuming that our lidar-derived estimates of transport are a reasonable baseline for comparison, our evaluation of bedload transport equations reaffirms that our ability to predict transport rates in steep settings remains poor. Although there is a mismatch between our lidar results, estimating bed material transport, and bed load transport equations, such a mismatch seems unlikely to account for the order-of-magnitude discrepancies they exhibit when compared to our lidar estimates and has no bearing on the inconsistency of the predictions when compared directly against each other. Although none of the examined equations appear to accurately capture transport process in Tahoma Creek across the range of observed flows, there is a slight improvement in transport predictions over the lower range of flows when the equations are used in conjunction with Mueller's formula for τ_{*c}. The critical shear stresses estimated by this formula are very similar to those we estimated through our stream gaging campaign, suggesting that the improvements observed are physically meaningful (Figure 12). The Recking equation uses a slope-dependent critical shear stress that was derived from the same data set used by *Mueller et al.* [2005], and both formulations provide similar results over the range of slopes observed in Tahoma Creek. Incorporation of an appropriate shear stress provides a plausible explanation for the (relative) success of the Recking equation compared to the Parker and Wilcock-Crowe equations. The Parker and Wilcock-Crowe equations both specify critical shear stresses that are much lower than those we estimated for Tahoma Creek and may explain some of the tendency of those equations to overpredict transport rates at low flows.

In contrast to the common wisdom that transport equations tend to overpredict transport rates in steep settings, our estimates of transport during the 2006 flood indicate that all equations significantly underpredicted transport rates during this extreme event. Although our estimates from a single stream over a single time period are obviously not conclusive, such a tendency would have implications for estimates of transport volumes integrated over long (decadal or longer) time scales, as well as the relative importance of extreme events. In the specific case of Tahoma Creek, the 3 days encompassing the 2006 flood are estimated to have accounted for around 80% of all the bed material transport over the 2002–2012 period and 50%–60% of all of the transport estimated to have occurred between 1943 and 2012. Compensating underpredictions and overpredictions may also lead to the incorrect conclusion that sediment transport equations performed well when compared against observations of temporally integrated transport, such as records of long-term sediment deposition in reservoirs. Without our temporally resolved estimates of transport, we would have likely arrived at similar conclusions, given the apparent success of several of the equations at predicting total transport volumes (Figure 9).

7. Conclusion

We presented an example of morphologic budgeting techniques used to estimate sediment fluxes in a steep mountain stream. Using three aerial lidar surveys of Tahoma Creek, Washington, we estimated accumulated sediment loads resulting from many transport events between 2002 and 2012, including a massive flood in 2006. We also presented a method by which two measurements of accumulated loads and the driving hydrology may be used to generate temporally resolved estimates of transport rates and provide a means of estimating transport rates outside of the survey period intervals. While this sequence of methods entails a number of assumptions, some inherent to the method and some specific to our study site, several lines of reasoning suggest we arrive at reasonable estimates of bed material transport in Tahoma Creek. Morphologic budgeting methods thus may present one potential way in which estimates of transport in steep fluvial setting may be obtained. The lack of agreement between our lidar-derived estimates of transport and those predicted from transport equations, as well as the lack of coherency between the various transport equation predictions, attests to the need for more such observations, particularly at higher flows.

Acknowledgments

The authors would like to acknowledge, first and foremost, the broad contributions of Paul Kennard, without whom this work would never have come about. Scott Beason generously provided field materials and help, including the capable hands of Corrie Floyd and Anna Snifter. General funding was provided through the National Park Service. This work has benefitted from the discussions and encouragements of Chris Magirl, Jon Nelson, Joe Walder, and Carolyn Driedger. The 2012 lidar data acquisition and processing was completed by the National Center for Airborne Laser Mapping (NCALM - http://www.ncalm.org). NCALM funding was provided by NSF's Division of Earth Sciences, Instrumentation and Facilities Program. EAR-1043051. http://dx.doi.org/10.5069/G9PZ56R1. Joe Wheaton, Adam Mosbruker, Nick Legg, and Jon Major all provided detailed and thoughtful reviews that have dramatically improved both the underlying material and the presentation of this manuscript.

References

Bathurst, J. C. (2007), Effect of coarse surface layer on bed-load transport, *J. Hydraul. Eng.*, *133*(11), 1192–1205, doi:10.1061/(ASCE)0733-9429(2007)133:11(1192).

Bunte, K., and S. Abt (2001), Sampling surface and subsurface particle-size distributions in wadable gravel-and cobble-bed streams for analyses in sediment transport, hydraulics, and streambed monitoring, *Gen. Tech. Rep. RMRS-GTR-74*, U.S. Department of Agriculture, Forest Service, Rocky Mountain Research Station.

Chiari, M., and D. Rickenmann (2007), The influence of form roughness on modelling sediment transport at steep slopes, in *Proceedings of the International Conference on Erosion and Torrent Control as a Factor in Sustainable River Basin Management* [CD-ROM], edited by S. Kostadinov, S. Bruk and D. Walling, Belgrade, Serbia.

Chiari, M., K. Friedl, and D. Rickenmann (2010), A one-dimensional bedload transport model for steep slopes, *J. Hydraul. Res.*, *48*(2), 152–160, doi:10.1080/00221681003704087.

Chiari, M., and D. Rickenmann (2011), Back-calculation of bedload transport in steep channels with a numerical model, *Earth Surf. Processes Landforms*, *36*(6), 805–815.

Croke, J., P. Todd, C. Thompson, F. Watson, R. Denham, and G. Khanal (2013), The use of multi temporal lidar to assess basin-scale erosion and deposition following the catastrophic January 2011 Lockyer flood, SE Queensland, Australia, *Geomorphology*, *184*, 111–126, doi:10.1016/j.geomorph.2012.11.023.

Curry, A. M., T. B. Sands, and P. R. Porter (2009), Geotechnical controls on a steep lateral moraine undergoing paraglacial slope adjustment, *Geol. Soc. Spec. Publ.*, *320*(1), 181–197, doi:10.1144/SP320.12.

Czuba, J. A., C. S. Magirl, C. R. Czuba, C. A. Curran, K. H. Johnson, T. D. Olsen, H. K. Kimball, and C. C. Gish (2012a), Geomorphic analysis of the river response to sedimentation downstream of Mount Rainier, Washington, *Open-File Report 2012-1242*, U.S. Geological Survey.

Czuba, J. A., T. D. Olsen, C. R. Czuba, C. S. Magirl, and C. C. Gish (2012b), Changes in sediment volume in Alder Lake, Nisqually River Basin, Washington, 1945–2011, *Open-File Report 2012-1068*, U.S. Geological Survey.

DeLong, S. B., C. S. Prentice, G. E. Hilley, and Y. Ebert (2012), Multitemporal ALSM change detection, sediment delivery, and process mapping at an active earthflow, *Earth Surf. Processes Landforms*, *37*(3), 262–272, doi:10.1002/esp.2234.

Fahnestock, R. K. (1963), Morphology and hydrology of a glacial stream—White River, Mount Rainier Washington, *Professional Paper 422-A*, U.S. Geological Survey.

Ferguson, R. I. (2003), The missing dimension: Effects of lateral variation on 1-D calculations of fluvial bedload transport, *Geomorphology*, *56*(1–2), 1–14, doi:10.1016/S0169-555X(03)00042-4.

Ferguson, R. I. (2007), Flow resistance equations for gravel- and boulder-bed streams, *Water Resour. Res.*, *43*(5), W05427, doi:10.1029/2006WR005422.

Fonstad, M. A., J. T. Dietrich, B. C. Courville, J. L. Jensen, and P. E. Carbonneau (2013), Topographic structure from motion: A new development in photogrammetric measurement, *Earth Surf. Processes Landforms*, *38*(4), 421–430.

Gomez, B., R. L. Naff, and D. W. Hubbell (1989), Temporal variations in bedload transport rates associated with the migration of bedforms, *Earth Surf. Processes Landforms*, *14*(2), 135–156.

Harding, D. (2004), Northern San Andreas Fault, CA and West Rainier Seismic Zone, WA LiDAR Metadata Report, *Tech. Rep.*, doi:10.5069/G9CC0XMC.

Iseya, F., and H. Ikeda (1987), Pulsations in bedload transport rates induced by a longitudinal sediment sorting: A flume study using sand and gravel mixtures, *Geogr. Ann. A.*, *69*, 15–27.

Kuhnle, R. A., and J. B. Southard (1988), Bed load transport fluctuations in a gravel bed laboratory channel, *Water Resour. Res.*, *24*(2), 247–260.

Lamb, M. P., W. E. Dietrich, and J. G. Venditti (2008), Is the critical Shields stress for incipient sediment motion dependent on channel-bed slope?, *J. Geophys. Res.*, *113*, F02008, doi:10.1029/2007JF000831.

Lane, S. N., R. M. Westaway, and D. Murray Hicks (2003), Estimation of erosion and deposition volumes in a large, gravel-bed, braided river using synoptic remote sensing, *Earth Surf. Processes Landforms*, *28*(3), 249–271, doi:10.1002/esp.483.

Lindsay, J. B., and P. E. Ashmore (2002), The effects of survey frequency on estimates of scour and fill in a braided river model, *Earth Surf. Processes Landforms*, *27*(1), 27–43.

McLean, D. G., and M. Church (1999), Sediment transport along lower Fraser River: 2. Estimates based on the long-term gravel budget, *Water Resour. Res.*, *35*(8), 2549–2559.

Meyer-Peter, E., and R. Müller (1948), Formulas for bed-load transport, *Proc. 2nd Congr. Int. Assoc. Hydraul. Res.*, Stockholm.

Milan, D. J., G. L. Heritage, A. R. Large, and I. C. Fuller (2011), Filtering spatial error from DEMs: Implications for morphological change estimation, *Geomorphology*, *125*(1), 160–171, doi:10.1016/j.geomorph.2009.03.021.

Mills, H. H. (1978), Some characteristics of glacial sediments of Mount Rainier, Washington, *J. Sediment. Res.*, *48*(4), 1345–1356.

Mills, H. H. (1979), Some implications of sediment studies for glacial erosion on Mount Rainier, Washington, *Northwest Sci.*, *53*(3), 190–199.

Mueller, E. R., J. Pitlick, and J. M. Nelson (2005), Variation in the reference shields stress for bed load transport in gravel-bed streams and rivers, *Water Resour. Res.*, *41*, W04006, doi:10.1029/2004WR003692.
NCALM (2012), Report for survey of southwest flanks of Mount Rainier, *Tech. Rep.*, doi:10.5069/G9PZ56R1.
Neill, C. R. (1971), River bed transport related to meander migration rates, *J. Waterway. Div.-Asce.*, *97*(4), 783–786.
Nitsche, M., D. Rickenmann, J. M. Turowski, A. Badoux, and J. W. Kirchner (2011), Evaluation of bedload transport predictions using flow resistance equations to account for macro-roughness in steep mountain streams, *Water Resour. Res.*, *47*, WO8513, doi:10.1029/2011WR010645.
Palt, S. M. (2001), Sedimenttransporte im Himalaya-Karakorum und ihre Bedeutung für Wasserkraftanlagen, PhD thesis, Institut für Wasserwirtschaft und Kulturtechnik, Karlsruhe.
Parker, G. (1990), Surface-based bedload transport relation for gravel rivers, *J. Hydraul. Res.*, *28*(4), 417–436, doi:10.1080/00221689009499058.
Pettyjohn, W. A., and R. Henning (1979), Preliminary estimates of groundwater recharge rates, related streamflow and water quality in Ohio, *Project Completion Report 552*, Dept. of Geology and Minerology, Ohio State Univ.
Popov, I. V. (1962), Application of morphological analysis to the evaluation of the general channel deformations of the River Ob, *Soviet Hydrol.*, *3*, 267–324.
Pratt-Sitaula, B., M. Garde, D. W. Burbank, M. Oskin, A. Heimsath, and E. Gabet (2007), Bedload-to-suspended load ratio and rapid bedrock incision from Himalayan landslide-dam lake record, *Quat. Res.*, *68*(1), 111–120, doi:10.1016/j.yqres.2007.03.005.
Recking, A. (2010), A comparison between flume and field bed load transport data and consequences for surface-based bed load transport prediction, *Water Resour. Res.*, *46*, W03518, doi:10.1029/2009WR008007.
Recking, A. (2013), Simple method for calculating reach-averaged bed-load transport, *J. Hydraul. Eng.*, *139*(1), 70–75, doi:10.1061/(ASCE)HY.1943-7900.0000653.
Recking, A., F. Liébault, C. Peteuil, and T. Jolimet (2012), Testing bedload transport equations with consideration of time scales, *Earth Surf. Processes Landforms*, *37*(7), 774–789.
Rickenmann, D. (2001), Comparison of bed load transport in torrents and gravel bed streams, *Water Resour. Res.*, *37*(12), 3295–3305.
Rickenmann, D., and A. Recking (2011), Evaluation of flow resistance in gravel-bed rivers through a large field data set, *Water Resour. Res.*, *47*, W07538, doi:10.1029/2010WR009793.
Robinson, J. E., T. W. Sisson, and D. D. Swinney (2010), Digital topographic map showing the extents of glacial ice and perennial snow-fields at Mount Rainier, Washington, based on the lidar survey of September 2007 to October 2008, *Data Series 549*, U.S. Geological Survey.
Schürch, P., A. L. Densmore, N. J. Rosser, M. Lim, and B. W. McArdell (2011), Detection of surface change in complex topography using terrestrial laser scanning: Application to the Illgraben debris-flow channel, *Earth Surf. Processes Landforms*, *36*(14), 1847–1859, doi:10.1002/esp.2206.
Scott, K. M., J. W. Vallance, and P. T. Pringle (1995), Sedimentology, behavior, and hazards of debris flows at Mount Rainier, Washington, *Survey Professional Paper 1547*, U.S. Geological Survey.
Sklar, L. S., and W. E. Dietrich (2004), A mechanistic model for river incision into bedrock by saltating bed load, *Water Resour. Res.*, *40*, W06301, doi:10.1029/2003WR002496.
Venditti, J. G., W. E. Dietrich, P. A. Nelson, M. A. Wydzga, J. Fadde, and L. Sklar (2010), Effect of sediment pulse grain size on sediment transport rates and bed mobility in gravel bed rivers, *J. Geophys. Res.*, *115*, F03039, doi:10.1029/2009JF001418.
Walder, J. S., and C. L. Driedger (1994a), Rapid geomorphic change caused by glacial outburst floods and debris flows along Tahoma Creek, Mount Rainier, Washington, USA, *Arct. Alp. Res.*, *26*(4), 319–327.
Walder, J. S., and C. L. Driedger (1994b), Geomorphic change caused by outburst floods and debris flows at Mount Rainier, Washington, with emphasis on Tahoma Creek valley, *Water-Resources Investigations Report 93-4093*, U.S. Geological Survey.
Wallick, J. R., J. E. O'Connor, S. W. Anderson, M. Keith, C. Cannon, and J. C. Risley (2010), Channel change and bed-material transport in the Umpqua River Basin, Oregon, *Open-File Report 2010-1314*, U.S. Geological Survey.
Watershed Sciences (2009), Lidar remote sensing data collection: Mount Rainier, WA, *Tech. Rep.*
Wheaton, J. M., J. Brasington, S. E. Darby, and D. A. Sear (2010), Accounting for uncertainty in DEMs from repeat topographic surveys: Improved sediment budgets, *Earth Surf. Processes Landforms*, *35*, 136–156, doi:10.1002/esp.1886.
Wilcock, P. R., and J. C. Crowe (2003), Surface-based transport model for mixed-size sediment, *J. Hydraul. Eng.*, *129*(2), 120–128, doi:10.1061/(ASCE)0733-9429(2003)129:2(120).
Williams, R. D., J. Brasington, D. Vericat, and D. M. Hicks (2013), Hyperscale terrain modelling of braided rivers: Fusing mobile terrestrial laser scanning and optical bathymetric mapping, *Earth Surf. Processes Landforms*, *39*, 167–183, doi:10.1002/esp.3437.
Yager, E. M., J. W. Kirchner, and W. E. Dietrich (2007), Calculating bed load transport in steep boulder bed channels, *Water Resour. Res.*, *43*, WO7418, doi:10.1029/2006WR005432.